Synthesis, Optoelectronic properties and Photovoltaic Performances of Wide Band-Gap Copolymers Based on Dibenzosilole and Quinoxaline units, Rivals to P3HT

Journal:	*Polymer Chemistry*
Manuscript ID	PY-ART-02-2016-000370.R2
Article Type:	Paper
Date Submitted by the Author:	02-May-2016

Complete List of Authors:	CAFFY, Florent; CEA, INAC-SPRAM; CNRS, INAC-SPRAM; Universite Grenoble Alpes, INAC-SPRAM DELBOSC, Nicolas; CEA, INAC-SPRAM; CNRS, INAC-SPRAM; Universite Grenoble Alpes, INAC-SPRAM Chavez, Patricia; ECPM LIPHT, Organic Chemsitry Lévêque, Patrick; UdS-CNRS, ICube FAURE-VINCENT, Jérôme; CEA, INAC-SPRAM; CNRS, INAC-SPRAM; Universite Grenoble Alpes, INAC-SPRAM TRAVERS, Jean-Pierre; CEA, INAC-SPRAM; CNRS, INAC-SPRAM; Universite Grenoble Alpes, INAC-SPRAM Djurado, David; CEA, INAC-SPRAM; CNRS, INAC-SPRAM; Universite Grenoble Alpes, INAC-SPRAM PECAUT, Jacques; CEA, INAC-SyMMES; Université Grenoble Alpes, INAC-SyMMES GREVIN, Benjamin; CEA, INAC-SPRAM; CNRS, INAC-SPRAM; Universite Grenoble Alpes, INAC-SPRAM LEMAITRE, Noëlla; CEA, LITEN-DTS-INES Leclerc, Nicolas; UdS-CNRS, LIPHT DEMADRILLE, Renaud; CEA, INAC-SPRAM; CNRS, INAC-SPRAM; Universite Grenoble Alpes, INAC-SPRAM

Polymer Chemistry

PAPER

Synthesis, Optoelectronic properties and Photovoltaic Performances of Wide Band-Gap Copolymers Based on Dibenzosilole and Quinoxaline units, Rivals to P3HT

Received 00th January 20xx,
Accepted 00th January 20xx

DOI: 10.1039/x0xx00000x

www.rsc.org/

F. Caffy[a,b,c], N. Delbosc[a,b,c], P. Chávez[d], P. Lévêque[e], J. Faure-Vincent[a,b,c], J.-P. Travers[a,b,c], D. Djurado[a,b,c], J. Pécaut[f,g], B. Grévin[a,b,c], N. Lemaitre[h], N. Leclerc[d], R. Demadrille[a,b,c]*.*

Three π-conjugated alternating copolymers, based on dibenzosilole as an electron-rich unit and fluorinated or non-fluorinated quinoxaline as an electron-withdrawing unit, connected through thiazole or thiophene moieties, have been synthesized, fully characterized and applied as a donor in polymer solar cells (PSCs). The three copolymers, namely **PDBS-TQx**, **PDBS-TQxF** and **PDBS-TzQx**, are belonging to wide band-gap semiconductors materials family, and they show an absorption edge in the visible close to 650 nm. In order to tune the position of the polymers energy levels, and in particular to decrease their HOMO energy level, we compare the use of thiazole spacer sandwiching the electron-deficient moiety as an alternative way to the popular backbone fluorination. PSCs based on a blend of **PDBS-TQx** and [6,6]-phenyl-C71-butyric acid methylester ($PC_{71}BM$) as an active layer have shown the best device performances with a maximum power conversion efficiency of 5.14% for the active area of 0.28 cm² (under standard illumination of AM 1.5G, 1000 W/m²). Interestingly this polymer outperform P3HT:($PC_{61}BM$) solar cells used as a reference material in this work. In addition to thorough characterization data, including among others spectroscopies, XRD, OFET, AFM and nc-AFM, we discuss in details the relationship between the chemical structures of the three polymers, their optoelectronic properties, the phase separation in blends with $PC_{71}BM$ and their photovoltaic performances.

Introduction

Polymer solar cells (PSC) are considered as a promising technology for renewable energy sources,[1] owing to their numerous advantages compared to other technologies employing inorganic semi-conductors. They have attracted the interest of many academic and industrial research teams[2] since it has been demonstrated that PSC can be manufactured on lightweight, flexible and biodegradable substrates[3] and that they can be deposited on a large area using printing technologies, which reduces the cost and the energy payback time of the solar cells.[4,5] In the last decade, with the goal to improve the attractiveness of PSC for future industrial production, many works have been focused on the development of more efficient devices by synthesizing new materials,[6,7] optimizing interface layers[8] and designing new device architectures.[9]

While conventional bulk-heterojunction devices based on narrow band-gap (NBG) polymers in a single cell are now grazing the theoretical PCE limit with efficiencies around 11%,[10–12] new approaches based on the multiple absorbing species such as multiple-junction architectures and ternary blend based devices have showed highly promising performances[13,14] with PCE records of 11.83% and 10.50% respectively.[15,16]

Tandem devices are fabricated by superposing vertically single bulk-heterojunction junction solar cells that are electronically connected by an appropriate recombination layer. This device architecture allows broadening the absorption spectra of the final devices by employing organic semiconducting materials with complementary absorption domains in the different sub-cells.

Ternary blend devices address the similar issue of a more efficient solar photon harvesting by using multiple absorbing species into a single active layer. Such a ternary solar cell can still benefit the easy fabrication process and has known a renewed interest in last years.[17,18]

For the fabrication of such panchromatic devices it exists a large variety of NBG materials that are capable to absorb visible and near-infra red light. Most of these polymers show PCE over 8% in single junction solar cells.[19–21] To the contrary,

[a] Univ. Grenoble Alpes, INAC-SPRAM, F-38000 Grenoble, France
[b] CNRS Alpes, INAC-SPRAM, F-38000 Grenoble, France
[c] CEA, INAC-SPRAM, F-38000 Grenoble, France
[d] Institut de Chimie et Procédés pour l'Energie, l'Environnement et la Santé (ICPEES), Univ. de Strasbourg, CNRS UMR 7515, 25 rue Becquerel, 67087 Strasbourg Cedex 2, France
[e] Laboratoire ICube, Univ. de Strasbourg, 23 rue du Loess, CNRS UMR 7357, 67037 Strasbourg Cedex 2, France
[f] Univ. Grenoble Alpes, INAC-SyMMES, F-38000 Grenoble, France
[g] CEA, INAC-SyMMES, F-38000 Grenoble, France
[h] CEA, LITEN, Département des Technologies Solaires, INES, 50 Avenue du Lac Léman 73375 Le Bourget du Lac, France

Electronic Supplementary Information (ESI) available. See DOI: 10.1039/x0xx00000x

the number of wide band-gap (WBG) materials capable to harvest photons at shorter wavelengths and showing sufficiently high performances for use in tandem or multi-junction devices is limited to few examples.[22–25]

To date, the most used WBG material in panchromatic devices is still the poly(3-hexylthiophene) (P3HT). This polymer when blended with fullerene derivatives [6,6]-phenyl-C61-butyric acid methyl ester ($PC_{60}BM$) or the indene-C60 bis-adduct ($IC_{60}BA$) can achieve PCE of 5%[22] and 6.5% respectively in single cell.[26] However P3HT has some limitations regarding the position of its highest occupied molecular orbital (HOMO) energy level that impedes to achieve high open circuit voltage (V_{OC}) in solar cells. Only few WBG polymers can outperform P3HT in the shorter wavelengths region (350 nm to 650 nm).[27,28] To improve the currently reported record efficiencies of tandem and multi-junction cells it is now essential to develop new WBG materials alternative to P3HT showing better photovoltaic performances. Ideally these materials should combine a wider band-gap (E_{opt} > 1.9 eV), a good mobility of the charge carriers in order to maximize the short-circuit current-density J_{sc}, and a low-lying HOMO energy level[29] that enables to achieve larger open circuit voltage (V_{OC}).

In this contribution, we report on the synthesis and the characterization of three wide band-gap copolymers (1.95 eV < E_{opt} < 2.00 eV) combining dibenzosilole and quinoxaline moieties. The quinoxaline and the dibenzosilole units were linked together either with a thiophene or a thiazole spacer to give the copolymers named **PDBS-TQx**, **PDBS-TQxF,** and **PDBS-TzQx**. The copolymers have been fully characterized optically and electronically prior to their use in bulk-heterojunction solar cells with fullerene derivatives. **PDBS-TQx**, **PDBS-TQxF**, that contain thiophene spacers, show relatively high hole mobility in field effect transistor configuration (OFET) with values ranging from $2.5x10^{-4}$ cm²/Vs up to $9x10^{-3}$ cm²/Vs. All the polymers revealed a quite narrow absorption in the visible range with an absorption edge close to 650 nm in solid state and a lower HOMO energy level than P3HT. The low-lying HOMO energy levels of these copolymers led to improved V_{OC} in solar cells compared to P3HT. After optimization of the processing conditions, we show that **PDBS-TQx**, when used in combination with $PC_{71}BM$, outperforms P3HT in BHJ solar cells leading to PCE up to 5.14% under standard illumination of AM 1.5G, 1000 W/m² (active area 0.28 cm²).

Results and discussion

Materials synthesis

As discussed in the introduction, the ideal WBG copolymer for BHJ solar cells should possess a low-lying HOMO energy level to ensure a high V_{OC} in solar cells. One useful method to control the HOMO and the lowest unoccupied molecular orbital (LUMO) energy levels of the donor materials is to design copolymers using electron-rich and electron-deficient units in order to build an alternating Donor-Acceptor structure.[30] Such D/A structures offer large possibilities to tune independently the HOMO and LUMO energy levels.[31] The combination of a weak donor segment and a medium to strong acceptor motif in the polymer backbone is a good strategy to maintain a low HOMO energy level and to achieve an intense absorption in the visible thanks to the internal charge transfer (ICT) absorption band.[30] For the preparation of our three copolymers, we have selected a quinoxaline[32] motif as electron-deficient unit and a dibenzosilole unit as electron-rich one. Dibenzosilole was chosen because of its high robustness compared to carbazole and fluorene units. Despite of quite similar electronic properties these moieties are known to undergo photo-oxidation processes upon light exposure leading to the degradation of their photovoltaic performances.[33,34]

The choice of the quinoxaline unit was related to the possibility to adjust its electro-withdrawing character by appropriate functionalizations either on the benzene or on the pyrazine ring.[35] Therefore to decrease the electron-withdrawing strength of the quinoxaline and to improve the solubility of the final polymers, two alkylthiophenes have been introduced on the pyrazine ring. Additionally we have investigated the effect of swapping H for F in the benzene ring of the quinoxaline on the materials properties. Fluorination is one of the most convenient and widely employed tools to fine-tune the energy levels and structural properties of copolymers.[36–38] Previous works have shown that the incorporation of fluorine atoms on the benzene ring of quinoxaline or benzothiadiazole decreases the HOMO energy levels of the corresponding polymers leading to increased V_{OC} of the PSC and increases the polymer crystallization and polymer domains purity.[37,39–41] Finally, we also investigated the use of thiazole spacer between D and A moieties instead of standard thiophene, as it has been shown recently that such modification could lead to a beneficial translation of both HOMO and LUMO levels towards deeper energy levels.[42] The copolymers synthesis requires first the preparation of a 5,5-dihexyl-3,7-bis-(4,4,5,5-tetramethyl-1,3,2-dioxaborolan-2-yl)-5H-dibenzo[b,d]silole precursor.[43] For the facile access to the polymers we have designed symmetric precursors containing a central quinoxaline unit flanked with the selected spacers (thiophene or thiazole). The copolymers can then be prepared from these monomers employing palladium-mediated cross-coupling polymerization conditions. The synthesis routes of the symmetric monomers are shown in Scheme 1. 4,7-di(thiophen-2-yl)benzo[c][1,2,5]thiadiazole **(1)**,[44] 1,2-bis(5-octylthiophen-2yl)ethane-1,2-dione **(2)**,[45] 1,4-dibromo-2,3-difluoro-5,6-dinitrobenzene **(3)**,[46] 4,7-di(thiazol-2-yl)benzo[c][1,2,5]thiadiazole **(5)**[47] were synthesized according to literature procedures. The target quinoxaline monomer **TQx** was obtained by reduction with zinc powder of the [1,2,5]-benzothiadiazole unit in **(1)** to give the corresponding diamino derivative that is later involved in a condensation reaction with the 1,2-bis(5-octylthiophen-2yl)ethane-1,2-dione. The bromination of the resulting molecule using N-bromosuccinimide (NBS) afforded the desired monomer **TQx-Br**. The analog of **TQx-Br**, *i.e.* **TzQx-Br** in which thiophene are replaced by thiazole rings, was prepared from 4,7-di(thiazol-2-yl)benzo[c][1,2,5]thiadiazole **(5)**[47] using the same procedures.

Finally, the fluorinated analogue of **TQxF-Br** was prepared in a slightly different manner. First, 1,4-dibromo-2,3-difluoro-5,6-dinitrobenzene was synthesized by nitration from 1,4-dibromo-2,3-difluorobenzene. Then 1,4-Bis(2-thienyl)-2,3-difluoro-5,6-dinitrobenzene **(4)** was obtained starting from compound **3** and tributyl(thiophen-2-yl)stannane using Stille coupling conditions.

Insert Scheme 1

The **TQxF** monomer was prepared by reduction of the nitro groups using Tin (II) chloride followed by a condensation on 1,2-bis(5-octylthiophen-2yl)ethane-1,2-dione **(2)**. This molecule was then brominated with NBS to afford the monomer **TQxF-Br**.

With all the monomers ready, the preparation of the three new D-A type copolymers **PDBS-TQx, PDBS-TQxF** and **PDBS-TzQx** was achieved by a Suzuki coupling polycondensation between the 5,5-dihexyl-3,7-bis(4,4,5,5-tetramethyl-1,3,2-dioxaborolan-2-yl)-5H-dibenzo[b,d]silole[43] and the corresponding dibromo-quinoxaline building blocks using $Pd_2dba_3/{}^tBu_3PHBF_4$ as catalyst. The synthetic conditions and the structures of the copolymers are shown in Scheme 2. The copolymers were obtained as purple solids with yields varying between 30% and 70%. After the synthesis, they were purified by precipitation and Soxhlet extraction with methanol, cyclohexane, and chloroform. They showed good solubility in common organic solvents such as chloroform, THF, and chlorobenzene. The molecular weights of the polymers were determined by Size Exclusion Chromatography (SEC) using tetrahydrofuran as eluent at 40°C and calibration with polystyrene standards. **PDBS-TQx**, **PDBS-TQxF,** and **PDBS-TzQx** revealed respectively an average molecular weight (M_n) of 48.8 $kg.mol^{-1}$, 34.2 $kg.mol^{-1}$ and 18.9 $kg.mol^{-1}$ and a polydispersity index (PDI) of 3.3, 2.5, and 2.2. The lower molecular weight of the thiazole derivative is assumed to come from the lower solubility of thiazole-based monomers.

Insert scheme 2

Optical properties of the copolymers

To further replace advantageously P3HT in tandem or ternary-based devices, the WBG materials should possess an intense absorption coefficient in the 350-650 nm region. UV-visible absorption spectra of the copolymers **PDBS-TQx**, **PDBS-TQxF** and **PDBS-TzQx** were recorded in chloroform solutions and in thin film casted from chlorobenzene solutions. The spectra are presented in Fig. 1a and 1b for the solution and thin films respectively, and the results are summarized in Table 2. The three polymers show quite similar in shape absorption spectra both in solution and in thin film. In solution they show a first maximum absorption peak in the UV part located between 381 nm and 406 nm corresponding to the π-π* transitions. They also possess a second peak that is clearly distinguished at longer wavelengths with a λ_{max} comprised between 526 nm and 546 nm. This second absorption band, typical in D-A chemical structures, corresponds to internal charge-transfer transitions (ICT) between the electron-rich and the electron-deficient segments.[48]

The absorption profiles of the three polymers are shifted toward longer wavelengths going from the solution to the solid state. In thin films, the maximum of the UV absorption peak is slightly red-shifted by 4 nm to 13 nm, whereas the peak corresponding to the ICT absorption is strongly shifted for all the polymers (by 19 nm for **PDBS-TQx**, 27 nm for **PDBS-TQxF** and 43 nm for **PDBS-TzQx)**. These behaviours indicate better delocalization of the electrons of the π-conjugated systems in solid state and they reflect that strong π-stacking interactions occur between polymer chains (see figure 1b). It could be noticed that all polymers present really similar absorption profiles with identical band-gap measured in solid state.

Insert figure 1

The photoluminescence spectra of the polymers were also recorded in solution and in thin films. We observed a strong shift of the emission peaks from circa 630 nm in solution to circa 720 nm in solid state (see Fig. S1). This shift is fully consistent with the better interactions between polymer chains in thin film.

Structural organization of the copolymers

Looking closer at the spectra, in addition to the larger bathochromic shifts observed for **PDBS-TQxF** and **PDBS-TzQx**, one can notice some features in the ICT absorption bands of these two polymers.

This may be an indication that these two polymers give rise to π-stacking interactions in solid state. To verify this hypothesis X-Ray diffraction experiments were carried out on casted polymer films. All polymers diffract rather weakly, but there are nevertheless distinct diffraction features in pure films that are detected. The presence, in all the diffractograms (see Fig.2), of one peak centred at 3.10-3.15 Å corresponds to the silicon substrate. All the three copolymers exhibit one Bragg peak centred in the 17-21 Å d-range which can fit well the periodic lateral distance between main chains. (Table 1).

Insert Figure 2

Insert Table 1

We also note the systematic presence of faint peaks localised between $21° < 2\theta < 25°$, corresponding to d-spacings of 4.23, 4.83 and 4.14 Å for **PDBS-TzQx**, **PDBS-TQxF** and **PDBS-TzQx**, respectively. These distances can be considered as average correlation distances separating first neighbour molecules in the direction perpendicular to the axis of the polymer backbone. These distances stay relatively large because of Van der Waals interactions of alkyl side groups preventing a closer packing of rigid conjugated flat chains. The study by X-ray diffraction measurements of single crystals of monomers DBS precursor as well as **TQx**, **TQxF-Br** and **TzQx-Br** has revealed

the planar structure of these different building blocks of the polymer backbones (see supporting information).
The crystal structures of the quinoxaline precursors show that the central unit and the thiophene or thiazole spacers are almost coplanar. The monomer **TQx** showed the highest planarity with dihedral angles between the central quinoxaline and the two adjacent thiophenes around 4.2° and 7.0°.
Insert Table 2

The quinoxaline unit substituted by fluorine atoms **TQxF-Br** shows slightly increased dihedral angles up to 4.7° and 10.0°. However, fluorine atoms give rise to stronger π-stacking interactions since the intermolecular distances between adjacent molecules is around 3.4 Å. The replacement of thiophene spacers by thiazole ones in **TzQx-Br** increased the dihedral angle values up to 8.9°. However the single crystal structure reveals also strong π- stacking interactions between thiazole rings with short intermolecular distances of circa 3.4 Å.
Finally, the type of X-ray profiles obtained for **PDBS-TQx** and for **PDBS-TQxF** are typical of layered structures exhibiting several orders of Bragg peaks of the same family. For these two polymers, layers of more or less regularly stacked chains can be reasonably assumed. The case of **PDBS-TzQx** is somewhat different because the presence of a doublet at low scattering angles is a strong indication of a more complex type of chain packing or orientation of the crystallites.

Electrochemical properties

Cyclic voltammetry (CV) of the polymers was carried out in a three-electrode cell using an Ag/AgCl reference electrode and a calibration with the ferrocene/ferrocenium (Fc/Fc^+) redox couple. The cyclic voltammetry curves are shown in Fig. 3a and the electrochemical data are summarized in Table 2. From the CV curves we found that the oxidation process occurred at 0.94V for **PDBS-TQx**, 1.09V for **PDBS-TQxF** and 1.31V for **PDBS-TzQx**. The onset of the reduction potentials of the polymers was found at -1.27V and -1.28V for **PDBS-TQx** and **PDBS-TQxF**, respectively but this value was shifted at -1.11V for **PDBS-TzQx**. From the ionisation potential and the electronic affinity measured by CV, the corresponding HOMO and LUMO energy levels were calculated using the following equations $E_{HOMO} = -(E_{OX} + 4.38)$ (eV) and $E_{LUMO} = -(E_{RED} + 4.38)$ (eV).[50] The HOMO energy level of **PDBS-TQx** was estimated at -5.32eV. The substitution of the quinoxaline unit with fluorine atoms in **PDBS-TQxF** induces a down-shift of the HOMO energy level at -5.47 eV. But, as expected, the strongest effect was observed when the thiophene spacers are replaced by thiazole units. Indeed the polymer **PDBS-TzQx** possess a HOMO energy level located at -5.69 eV. On the contrary, the impact of the different chemical variations on the LUMO levels is relatively weak. **PDBS-TQx** and **PDBS-TQxF** have a LUMO levels located at circa -3.10 eV and **PDBS-TzQx** shows a LUMO level at -3.27 eV. Interestingly all the polymers have a HOMO energy level deeper than the one of P3HT (E_{HOMO} = -4.90 eV)[51,52] (see Figure 3b). This feature is expected to give rise to higher open circuit voltage for the solar cells.

Insert Figure 3

Theoretical calculations

In order to investigate the intrinsic difference between the polymers and to better understand how the chemical modifications influence the energy levels positions and the electron density distribution, theoretical calculations were performed by Density Functional Theory using the B3LYP hybrid method. To simplify the calculation, only one set of repeating units of each polymer was used for the calculation and the long alkyl chains were replaced by methyl groups. The optimisation of the geometry was carried out with the data of each monomer deduced from the single crystal X-Ray diffraction. The simulated electron density distribution and the HOMO and LUMO energy levels with the optimized geometry are shown in Fig. 4.

The calculated HOMO energy levels of **PDBS-TQx**, **PDBS-TQxF** and **PDBS-TzQx** were -5.27 eV, -5.38 eV and -5.57 eV respectively. The calculated LUMO energy levels of **PDBS-TQx**, **PDBS-TQxF** and **PDBS-TzQx** were -2.80 eV, -2.83 eV and -3.05 eV respectively. These values are quite consistent with the experimental ones found from electrochemical measurements. As expected, the three polymers show an electron density distribution of the LUMO energy levels mainly located on the quinoxaline moiety, which is the most electro-deficient unit in the polymer backbone. However we found that the electron density of the HOMO energy level of **PDBS-TQx** is rather delocalized on the aromatic cores of the polymer backbone including the benzene ring of the quinoxaline. The fluorine substitutions on **PDBS-TQxF**, that make the quinoxaline unit more electron deficient, slightly transferred the electron density of the HOMO energy level on the dibenzosilole unit. Finally the use of thiazole spacers in **PDBS-TzQx** induces a similar effect and increases the contribution of dibenzosilole to the HOMO energy level.

Insert figure 4

Electronic transport properties

The charge carrier mobility of the donor polymer is an important parameter that partly governs the performances of BHJ solar cells. A high charge carrier mobility may contribute to improve the J_{sc} and the Fill Factor (FF) leading to a higher PCE. The hole mobility of the copolymers were measured in organic field-effect transistors (OFETs) with a bottom gate and bottom contact configuration. The OFETs characteristics are presented in table 3. **PDBS-TQx** exhibits a hole mobility of 3.0 x 10^{-4} $cm^2.V^{-1}.s^{-1}$. Swapping H to F in the quinoxaline unit allows to increase the hole mobility of **PDBS-TQxF** up to 1.0 x 10^{-3} $cm^2.V^{-1}.s^{-1}$. After thermal annealing a highest value of 4.5 x 10^{-3} $cm^2.V^{-1}.s^{-1}$ was achieved in the linear regime and this value

rises at 6.5 x 10^{-3} $cm^2.V^{-1}.s^{-1}$ in the saturated regime (see supporting information). The lower hole mobility of (*circa* one order of magnitude) measured for the **PDBS-TzQx** polymer compared to the polymers **PDBS-TQxF** and **PDBS-TQx** could be attributed to i) the lower ordering of the polymer chains in thin films ii) the **PDBS-TzQx** macromolecular parameters including shorter polymer chains (**PDBS-TQx** M_n = 48.8 $kg.mol^{-1}$, and **PDBS-TQxF** M_n = 34.2 $kg.mol^{-1}$ vs **PDBS-TzQx** M_n = 18.9 $kg.mol^{-1}$). Indeed it is well-known that the chain length of the deposited polymers is a determining factor in the fabrication of layers with high carriers mobility. High M_w fractions can lead to improved charge transport properties by increasing the conjugation length, the probability of the inter-chain charge carriers hopping and by improving the connectivity between domains.[53–55] The rather good hole mobility value for the polymers **PDBS-TQxF** may originate from larger crystal size that are usually observed with fluorinated copolymers, probably due to increased π-stacking interactions[56].

Insert table 3

Photovoltaic properties

To illustrate the potential of these copolymers for use in photovoltaic devices, thin-film BHJ solar cells with the standard device architecture ITO/PEDOT:PSS /polymer:$PC_{71}BM$/Ca/Al (active area 0.28 cm^2, masked) were fabricated and tested under AM 1.5G, solar illumination at 1000 $W.m^{-2}$. Several parameters such as the Donor-Acceptor ratio, the thickness of the active layer, the use of additives and the thermal post-treatment of the thin films were investigated. The results were compared to optimized reference P3HT-$PC_{61}BM$ solar cells measured under the same conditions and to state of the art P3HT-$PC_{71}BM$ solar cell reported by Sakai and co-workers.[57] Various solvents and additives have been reported in the literature in order to improve the solar cell efficiencies. In this study chlorobenzene, o-dichlorobenzene and *para*-xylene were tested as solvent and di-iodo-octane (DIO) and anisole were evaluated as additive to deposit the polymer:$PC_{71}BM$ mixture.[58] (See Table S2). For this class of polymers, it was systematically found that, chlorobenzene with 3 % of DIO for the processing, gives the better performances in photovoltaic devices. The improvement of the PCE was mainly originating from a much higher short circuit current density (J_{sc}) and a higher fill factor (FF). This observation can be rationally explained by studying the morphology of the active layers employing atomic force microscopy (AFM) in the Tapping Mode. (See figure S4). Indeed it was found a strong dependency of the morphology of the blends depending on the processing conditions. The use of DIO as additive reduces the size of the domains and give rise to a much better structuration of the two percolating networks and a higher homogeneity of the film.[59,60]

The thickness of the active layers was also optimized by analysing its influence on the performances of the devices (the thickness was varied between 50 nm and 160 nm). The photovoltaic data are shown in ESI. For all the polymers the optimum thicknesses were found between 50 and 75 nm.

Insert table 4

Fig. 5 shows the representative current density–voltage (*J*–V) curves of the three polymers in optimized device configuration, and their detailed photovoltaic parameters are summarized in Table 4.

Among the three polymers of this study, the best performances were achieved with **PDBS-TQx**, a V_{OC} of 0.85 V, a J_{SC} of 9.72 $mA.cm^{-2}$, a FF of 0.62 and a PCE of 5.14% were obtained for the best cell with this polymer and an average PCE of 4.93 % was demonstrated over 5 cells. For this polymer a post-fabrication thermal annealing treatment was not effective to improve the performances. These results highlight the higher performances of **PDBS-TQx**, compared to P3HT in solar cells.

Insert figure 5

The improvement mostly originates from the higher V_{OC} of the solar cells fabricated with this material which is higher by 0.2 V compared to P3HT.

The substitution of the quinoxaline with fluorine atoms in **PDBS-TQxF** has a significant effect on the performances. For this polymer the best cell revealed a V_{OC} of 0.81 V, a J_{SC} of 7.27 $mA.cm^{-2}$, a FF of 0.51 leading to a PCE of 2.98%. It should however be noticed that after thermal annealing at 120°C, the performances increased to reach a PCE of 3.19% with a V_{OC} of 0.76 V, a J_{SC} of 7.61 $mA.cm^{-2}$ and a FF of 0.55.

The performances of the solar cells containing the thiazole-based copolymer **PDBS-TzQx** were the lowest. In this case the overall operating parameters are decreased to reach a V_{OC} of 0.63 V, a FF of 0.41 and a J_{SC} of 4.92 $mA.cm^{-2}$ leading to a maximum PCE of 1.27%. As for **PDBS-TQx**, a thermal annealing of the devices did not yield higher performances. The much lower J_{SC} and FF for the **PDBS-TzQx**-based devices can be explained by its lower charge carriers mobility as demonstrated earlier. However the origin of the drop in the V_{OC} value is not yet fully understood.

Film morphology

The morphology of the polymer:$PC_{71}BM$ blend films with the optimized weight ratio was investigated by tapping-mode atomic force microscopy (AFM). The AFM topographic images are shown in fig. 6. The morphology of pristine polymers with $PC_{71}BM$ shows aggregated domains with diameters around 500 nm for **PDBS-TQx**, 300 nm for **PDBS-TQxF** and 260 nm for **PDBS-TzQx**. (Fig. 6 a-c-e) This type of phase segregation is expected to be responsible for the enhanced exciton recombination and the dramatic drop of the current density when the polymers are processed without additives. This morphology also explains why our attempts to improve the morphology of the donor–acceptor networks by a simple thermal treatment were not successful. As explained before,

with the goal to enhance the miscibility of the two components and to favour the formation of a better interpenetrating donor–acceptor network, we used DIO as a processing additive. DIO is widely used to enable morphological control in bulk heterojunction materials where thermal annealing is either undesirable or ineffective. When used in small amount, it can increase the relative solubility of the fullerene compared to the polymer and it ensures that the two materials are well-solubilized in the processing solution.[59]
The AFM morphology images confirmed that the aggregates sizes decreased after adding DIO and each blend appears more homogeneous (Fig. 6 b-d-f). Consequently, better photovoltaic properties are obtained with these blends. However due to the limited resolution of the technique it is difficult to confirm that the two types of domains visible in the AFM images correspond to pure materials, they could also correspond to inter-mixed phases.[61]

Insert Figure 6

Insert Figure 7

To investigate more in details the morphology of the active area of our champion cell, i.e **PDBS-TQx**:$PC_{71}BM$ we used non-contact AFM (nc-AFM) under ultra-high vacuum.[62] In topography (Fig. 7a) a fine phase separation is clearly visible. The analysis of the damping images (Fig. 7b) revealed a more complex phase structuration. Besides a nano-phase segregation at the 10 nm scale, larger features appear at the 100nm scale. These data show that, despite the nanometer-scale phase segregation, the relative concentration of the donor and acceptor components varies at the mesoscopic scale. This strongly suggests that further improvement can be expected by achieving an even more homogeneous blend morphology.[61]

Recombination kinetics

An important parameter in the performance of the bulk heterojunction solar cells is the charge recombination kinetics, which can be studied by analysing the light intensity dependence.[63–65] Light-intensity-dependent J–V characteristics of the **PDBS-TQx**:$PC_{71}BM$ and **PDBS-TQxF**:$PC_{71}BM$ blends polymers were measured. This experiment was carried out in order to shed light on the fundamental processes that make **PDBS-TQx**-based devices performances better than the ones of the devices based on **PDBS-TQxF**. Light intensity from 100 to 9 $mW.cm^{-2}$ were employed and the *J*-V characteristics of the devices based on **PDBS-TQx** are shown in the fig. 8a and those for **PDBS-TQxF** based devices are shown in the fig. 8b.

Insert Figure 8

For the devices based on **PDBS-TQx**, the photocurrent quickly saturated at low reverse bias, on the contrary, for the devices based on **PDBS-TQxF** the photocurrent saturation is only observed at high reverse bias as evidenced especially at high illumination. This behavior could be explained by more charge carrier recombination for the devices based on **PDBS-TQxF**, especially for voltages approaching the V_{OC}. Figure 9 shows the variation of the J_{SC} as a function of light intensity for the solar cells based on **PDBS-TQx**:$PC_{71}BM$ and **PDBS-TQxF**:$PC_{71}BM$.
In organic solar cells, the dependence of the steady state short circuit current density J_{SC} as a function of the incident light intensity (I) can be expressed according to a power law $J_{SC} \infty I^{\alpha}$. The physical interpretation of the fitting parameter α is still under debate since it does not give a high-precision measure of the recombination mechanism. However, a fitting parameter α close to 1 is often attributed to a first order loss process whereas a value close to 0.5 is related to a second order (bimolecular) loss process. In other words when the α value is close to the unity it corresponds to a low bimolecular recombination rate.[66,67] Herein, in both devices investigated, the α values are close to unity, which indicates that monomolecular recombination is the dominant loss mechanism.
In organic solar cells, the nature of the main recombination process (monomolecular versus bimolecular) can also be determined by the slope of V_{OC} versus ln(I). Figure 10 displays the V_{OC} as a function of the light intensity for the solar cells based on **PDBS-TQx**:$PC_{71}BM$ and **PDBS-TQxF**:$PC_{71}BM$. A slope of 2 kT/q is observed in case of monomolecular recombination where k is the Boltzmann constant, T the temperature and q the elementary charge. For bimolecular recombination, a slope of kT/q is observed.[66]

Insert Figure 9

Insert Figure 10

In our case, the slope values for the solar cells based on **PDBS-TQx** and **PDBS-TQxF** are equal to 1.29 kT/q and 1.63 kT/q, respectively. This result indicates that monomolecular recombination seems even more pronounced with our fluorinated copolymer, i.e. **PDBS-TQxF**. Opposite effects have been reported on other class of fluorinated copolymers containing benzothiadiazole units such as PCPDTBT.[68] Therefore it seems that the introduction of fluorine substituents on the electron-withdrawing units do not lead systematically to a decrease in the charge recombination process.

Conclusions

In summary, the synthesis, the characterization of the optoelectronic properties, the structural organization and the photovoltaic properties of a series of wide band gap copolymers based on dibenzosilole and fluorinated or non-fluorinated quinoxaline sub-units connected through thiophene or thiazole segments are described. The copolymers, namely **PDBS-TQx**, **PDBS-TQxF** and **PDBS-TzQx** present an absorption edge close to 650 nm in the solid state and HOMO energy levels comprised between -5.3 eV and -5.7

eV. When they are combined to $PC_{71}BM$ to fabricate bulk-heterojunction solar cells, PCE ranging from 1.27% to 5.14% are achieved. Interestingly one of the new polymers, i.e. **PDBS-TQx** leads to increased V_{oc} (by circa 0.2V) and superior solar cell performances compared to a benchmark cell based on P3HT, one of the most known wide band gap polymers in the field. Contrary to P3HT, it is important to mention here that record performances with **PDBS-TQx** were obtained without any post-fabrication treatment such as thermal or solvent annealing. Despite a higher hole mobility and a deeper HOMO energy level, **PDBS-TQxF** performances in solar cells only reached 3.19%. By using experimental photocurrent measurement in combination with light intensity dependence, the lower efficiency of **PDBS-TQxF** is attributed to a higher monomolecular charge recombination rate.

Owing to the opto-electronic properties of **PDBS-TQx** and the quite promising performances in single bulk-heterojunction junction solar cells, we believe that this material could be valuable to develop tandem devices or ternary blend devices where the complementary of the absorption domains of the different components is essential to achieve record performances.

Experimental section

Instrumentation

^{1}H, ^{19}F and ^{13}C NMR spectra were recorded in chloroform-d solutions on a Brucker AC200 or Brucker AC400 spectrometers. Elemental analyses (C, H, N and S) and mass spectroscopy measurements were carried out by CRMPO at the University of Rennes 1 (France). The molecular weight was measured by IPCM at the Sorbonne University and polystyrene was used as the standard (THF as eluent). Cyclic voltammetry of polymer films were measured against Ag/AgCl as the reference electrode, Pd as counter electrode and Pt as working electrode in a 0.2M electrolyte containing tetrabutylammonium hexafluoro-phosphate in acetonitrile.

Materials Synthesis

All chemicals were purchased from Aldrich, Acros organics, Strem Chemicals, Alfa Aesar, Fluorochem or TCI Chemicals, and used without further purification. Solvent tetrahydrofuran was distilled over sodium-benzophenone under an atmosphere of dry argon prior to use.

4,7-di(thiophen-2yl)benzo[c][1,2,5]thiadiazole (1)

4,7-dibromobenzo[c][1,2,5]thiadiazole (2.00 g, 6.80 mmol), 2-thienylboronic acid (2.32 g, 17.69 mmol) and Tétrakis-(triphenylphosphine)-palladium (393 mg, 340 µmol) were solubilised in toluene (10 mL) and dried THF (10mL) under argon. A 2M solution of K_2CO_3 in water was degased by bubbling argon in it during 1 hour, before adding 8.84 mL (17.69 mmol). Then 2 drops of Aliquat 336 were added, and the flask was deeped in a thermostated oil bath at 90°C and kept under argon. The reaction was monitored by TLC. After 48 hours, the temperature was decreased to room temperature. Water was added and organic compounds were extracted by Et_2O. The organic layer was washed by water, dried over $MgSO_4$ and concentrated. The desired compound was purified by chromatography over silica with 50 % of $CHCl_3$ in C_6H_{14} as eluent. The red solid powder was recrystallized in ethanol. Finally, compound 1 was obtained as red needles (1.21 g, 60%). ^{1}H NMR ($CDCl_3$, 200 MHz, δ): 8.12 (dd, *J* = 3.8 Hz, *J* = 1.2 Hz, 2H), 7.88 (s, 2H), 7.46 (dd, *J* = 5.2 Hz, J = 1.2 Hz, 2H), 7.22 (dd, *J* = 5.2 Hz, *J* = 3.8 Hz, 2H). MS: calcd, 300.99279; found, 300.9928.

1,2-bis(5-octylthiophen-2yl)ethane-1,2-dione (2)

2-*n*-octylthiophene (5.00 g, 25.46 mmol) was solubilised in dried tetrahydrofuran (THF) (20 mL) at -78°C under argon. Then *n*-butyllithium (11.20 mL, 28.01 mmol, 2.5M in hexane) was added dropwise. Temperature was kept between -78°C and -50°C during 2 hours. This mixture was added dropwise on a solution of LiBr (2.21 g, 25.46 mmol) and CuBr (3.65 g, 25.46 mmol) in dried THF (65 mL) at -78°C under argon. After 15 minutes oxalylchloride (1.45 g, 11.46 mL) was added dropwise. The reaction temperature slowly increased to room temperature. After 2.5 hours the reaction was quenched by adding a saturated aqueous solution of NH_4Cl. The organic compound was extracted by Et_2O, washed by saturated aqueous solution of NaCl, dried over $MgSO_4$ and concentrated. The solid powder was recrystallized in hexane, deeped in liquid nitrogen and filtered. Finally, compound 2b was obtained as a yellow solid (4.46 g, 68%). ^{1}H NMR ($CDCl_3$, 200 MHz, δ): 7.86 (d, *J* = 3.8 Hz, 2H), 6.88 (d, *J* = 3.8 Hz, 2H), 2.88 (t, *J* = 7.4 Hz, 4H), 1.72 (m, 4H), 1.27 (m, 20H), 0.88 (m, 6H); ^{13}C NMR ($CDCl_3$, 50 MHz, δ): 182.6, 160.0, 137.7, 136.5, 126.4, 31.8, 31.3, 30.8, 29.2, 29.1, 29.0, 22.6 and 14.1. MS: calcd, 447.23915; found, 447.2397.

2,3-bis(5-octylthiophen-2-yl)-5,8-di(thiophen-2-yl)Quinoxaline (TQx)

4,7-di(thiophen-2-yl)benzo[c][1,2,5]thiadiazole (0.26 g, 0.86 mmol) and zinc dust (0.68 g, 10.00 mmol) were added to a mixture of acetic acid (20 mL), ethanol (5 mL) and water (5 mL) and heated to 100°C under nitrogen for 4 hours. The insoluble solid was then removed by filtration and the filtrate was added to 1,2-bis(5-octylthiophen-2-yl)ethane-1,2-dione (0.35 g, 0.78 mmol). The mixture was heated at 70°C for 15 h. The organic compound was concentrated and purified by chromatography over silica with 20 % of CH_2Cl_2 in C_6H_{14} as eluent. Finally, TQx was obtained as an orange solid (340 mg, 63%). ^{1}H NMR ($CDCl_3$, 400 MHz, δ): 8.02 (s, 2H), 7.88 (dd, *J* = 3.6 Hz, *J* = 1.0 Hz, 2H), 7.53 (dd, *J* = 5.2 Hz, *J* = 1.0 Hz 2H), 7.41 (d, *J* = 3.6 Hz, 2H), 7.19 (dd, *J* = 5.2 Hz, *J* = 3.6 Hz, 2H), 6.72 (d, *J* = 3.6 Hz, 2H), 2.89 (t, *J* = 8 Hz, 4H), 1.76 (m, 4H), 1.5-1.2 (m, 20H), 0.89 (m, 6H); ^{13}C NMR ($CDCl_3$, 101 MHz, δ): 150.9, 144.8, 139.2, 138.8, 136.4, 130.7, 130.0, 128.3, 126.9, 126.7, 126.7, 124.6, 31.8, 31.5, 30.4, 29.3, 29.2, 29.2, 22.6 and 14.1. Anal. Calcd for $C_{40}H_{46}N_2S_4$: C, 70.34; H, 6.79; N, 4.10; S, 18.77. Found: C, 70.30; H, 6.81; N, 4.02; S, 18.60. MS: calcd, 683.26166; found, 683.2617.

5,8-bis(5-bromothiophen-2-yl)-2,3-bis(5-octylthiophen-2-yl)Quinoxaline (TQx-Br)

N-bromosuccinimide (177 mg, 0.99 mmol) was added on a solution of 2,3-bis(5-octylthiophen-2-yl)-5,8-di(thiophen-2-yl)quinoxaline (340 mg, 0.50 mmol) in $CHCl_3$ (20 mL) and acetic acid (3 mL) at 0°C. The temperature slowly increased to room temperature. After 15 hours, the organic compound was concentrated and purified by chromatography over silica with 20 % of $CHCl_3$ in C_6H_{14} as eluent. Finally, TQx-Br was obtained as an orange solid (348 mg, 83%). ^{1}H NMR ($CDCl_3$, 400 MHz, δ): 7.83 (s, 2H), 7.48 (d, *J* = 4.0 Hz, 2H), 7.38 (d, *J* = 3.7 Hz, 2H), 7.08 (d, *J* = 4.0 Hz, 2H), 6.72 (d, *J* = 3.7 Hz, 2H), 2.91 (t, *J* = 7.6 Hz, 4H), 1.84-1.73 (m, 4H), 1.51-1.23 (m, 20H), 0.90 (t, *J* = 6.8 Hz, 6H); ^{13}C NMR ($CDCl_3$, 101 MHz, δ): 151.3, 145.1, 139.6, 138.6, 135.7, 130.2, 129.9, 129.1, 125.7, 125.5, 124.6, 116.5, 31.8, 31.4, 30.4, 29.3, 29.2, 29.1, 22.6 and 14.1. Anal. Calcd for $C_{40}H_{44}N_2S_4Br_2$: C, 57.14; H, 5.27; Br, 19.01; N, 3.33; S, 15.25. Found: C, 57.01; H, 5.33; N, 3.17; S, 14.90. MS: calcd, 839.08268; found, 839.0826.

1,4-Bis(2-thienyl)-2,3-difluoro-5,6-dinitrobenzene (4)

1,4-dibromo-2,3-difluoro-5,6-dinitrobenzene (400 mg, 1.10 mmol), 2-tributylstannyl-thiophene (0.77 mL, 2.42 mmol) and tetrakis-(triphenylphosphine)-palladium (63.9 mg, 0.055 mmol) were put in a schlenk, and purged with argon. Then, anhydrous toluene (20 mL) was added. The schlenk was deeped in a thermostated oil bath at 95°C and kept under argon for 72 hours. Then, the solvent was removed and the residue was purified by chromatography over silica with 25% of dichloromethane in C_6H_{14} as eluent. Finally, compound 4 was obtained as a yellow powder (348 mg, 85%). ^{1}H NMR (Acetone d_6, 200 MHz, δ): 7.92 (dd, *J* = 5.1 Hz, *J* = 1.2 Hz, 2H), 7.40 (dd , *J* = 3.6 Hz, *J* = 1.2 Hz, 2H), 7.29 (dd, *J* = 5.1 Hz, *J* = 3.6Hz, 2H); ^{13}C NMR ($CDCl_3$, 101 MHz, δ): 150.3 (d), 147.7 (d), 130.7, 130.4, 128.0 and 125.0; ^{19}F NMR ($CDCl_3$, 376 MHZ, δ): -125.7 (s). Anal. Calcd for $C_{14}H_6F_2N_2O_4S_2$: C, 45.65; H, 1.64; F, 10.32; N, 7.61; O, 17.37; S, 17.41. Found: C, 45.97; H, 1.76; N, 7.20; S, 18.54. MS: calcd, 368.98153; found, 368.9811.

6,7-difluoro-2,3-bis(5-octylthiophen-2-yl)-5,8-di(thiophen-2-yl)Quinoxaline (TQxF)

1,4-Bis(2-thienyl)-2,3-difluoro-5,6-dinitrobenzene (200 mg, 0.54 mmol) was solubilised in ethanol (10 mL) and aqueous solution of hydrochloric acid 30% (4 mL). The flask was deeped in a themostated oil bath at 70°C. Then, tin(II)chloride (618 mg, 3.26 mmol) was added. After 1.5 hour, the temperature is slowly decreased to room temperature. Then $CHCl_3$ (8 mL) and aqueous solution of NH_3 28% (3.2 mL) were added. The mixture was stirred 1.5 hour at room temperature. Then, the organic compound was extracted by $CHCl_3$, washed by a 0.5M aqueous solution of NaOH, washed by water, dried over $MgSO_4$ and concentrated. The orange compound obtained was solubilised in acetic acid (10 mL) under argon, then 1,2-bis(5-octylthiophen-2-yl)ethane-1,2-dione (242 mg, 0.54 mmol) was added. The flask was deeped in a thermostated oil bath at 70°C. After 18 hours, the temperature was decreased to room temperature. Water was added and organic compounds were extracted by CH_2Cl_2. The organic layer was washed by water, dried over $MgSO_4$ and concentrated. The desired compound was purified by chromatography over silica with 20 % of $CHCl_3$ in C_6H_{14} as eluent. Finally, TQxF was obtained as a yellow solid (153 mg, 40%). ^{1}H NMR ($CDCl_3$, 400 MHz, δ): 8.01 (dd, *J* = 3.6 Hz, *J* = 1.0 Hz, 2H), 7.66 (d, *J* = 5.2 Hz, *J* = 1.0 Hz 2H), 7.41 (d, *J* = 3.6 Hz, 2H), 7.25 (dd, *J* = 5.2 Hz, *J* = 3.6 Hz 2H), 6.72 (d, *J* = 3.6 Hz, 2H), 2.88 (t, *J* = 8.0 Hz, 4H), 1.75 (quint, *J* = 7.6 Hz, 4H), 1.5-1.2 (m, 20H), 0.89 (m, 6H); ^{13}C NMR ($CDCl_3$, 101 MHz, δ): 151.2, 138.4, 130.9, 130.8, 130.8, 130.7, 130.2, 129.7, 126.5, 124.7, 31.9, 31.5, 30.4, 29.3, 29.3, 29.2, 22.7 and 14.1; ^{19}F NMR ($CDCl_3$, 376 MHZ, δ): -129.8 ppm (s). Anal. Calcd for $C_{40}H_{44}N_2S_4F_2$: C, 66.82; H, 6.17; F, 5.28; N, 3.90; S, 17.83. Found: C, 66.87; H, 6.11; N, 3.64; S, 17.64.

5,8-bis(5-bromothiophen-2-yl)-6,7-difluoro-2,3-bis(5-octylthiophen-2-yl)Quinoxaline (TQxF-Br)

N-bromosuccinimide (74 mg, 0.42 mmol) was added on a solution of 6,7-difluoro-2,3-bis(5-octylthiophen-2-yl)-5,8-di(thiophen-2-yl)quinoxaline (150 mg, 0.21 mmol) in $CHCl_3$ (10 mL) and acetic acid (1.5 mL) at 0°C. The temperature slowly increased to room temperature. After 15 hours, the organic compound was concentrated and purified by chromatography over silica with 20 % of $CHCl_3$ in C_6H_{14} as eluent. Finally, TQxF-Br was obtained as an orange solid (165 mg, 90%). ^{1}H NMR ($CDCl_3$, 400 MHz, δ): 7.69 (d, *J* = 4.1 Hz, 2H), 7.36 (d, *J* = 3.7 Hz, 2H), 7.11 (d, *J* = 4.1 Hz, 2H), 6.72 (d, *J* = 3.7 Hz, 2H), 2.90 (t, *J* = 7.6 Hz, 4H), 1.78 (m, 4H), 1.5-1.2 (m, 20H), 0.90 (m, 6H); ^{13}C NMR ($CDCl_3$, 101 MHz, δ): 151.7, 149.3 (dd, $^1J_{CF}$ = 258.5 Hz, $^2J_{CF}$ = 19.0 Hz), 144.9, 138.0, 133.1, 132.4, 130.8, 130.5, 129.2, 124.8, 118.5, 116.7, 31.9, 31.5, 30.5, 29.4, 29.3, 29.2, 22.7 and 14.2; ^{19}F NMR ($CDCl_3$, 376 MHZ, δ): -129.4 ppm (s). Anal. Calcd for $C_{40}H_{42}N_2S_4F_2Br_2$: C, 54.79; H, 4.83; Br, 18.23; F, 4.33; N, 3.19; S, 14.63. Found: C, 54.91; H, 4.90; N, 3.14; S, 14.65. MS: calcd, 875.06384; found, 839.0636.

4,7-Di(thiazol-5-yl)benzo[c][1,2,5]thiadiazole (5)

4,7-dibromobenzo[c][1,2,5]thiadiazole (0.50 g, 1.70 mmol), Pd-Herrmann (0.08 g, 0.08 mmol), 3,4,5,6-tetramethyl-t-Bu-X-Phos (0.08 g, 0.51 mmol), Cs2CO3 (1.22 g, 3.74 mmol), and PivOH (0.05 g, 0.51 mmol) were put in a Schlenk under argon. Dried DMAc (10 mL) was added followed by thiazole (0.29 g, 3.40 mmol). The Schlenk tube was dipped in a thermostated oil bath at 120°C. After 16 hours, the temperature was decreased to room temperature. The organic compound was extracted with CH_2Cl_2, washed with water and dried with Na_2SO_4. The organic layer was concentrated. The desired compound was purified by chromatography over silica with 10 % of EtOAc in CH_2Cl_2 as eluent followed by a recrystallization in $CHCl_3$/methanol. Finally, compound 5 was obtained as an orange solid (0.39 g, 75 %). ^{1}H NMR ($CDCl_3$, 300 MHz): δ (ppm): 8.92 (s, 1H), 8.82 (s, 1H), 7.87 (s, 1H). ^{13}C NMR ($CDCl_3$, 75 MHz): δ (ppm): 154.0, 152.3, 142.9, 134.0, 126.8, 124.2. MS: calcd, 302.9827; found, 302.9842.

2,2'-(2,3-bis(5-octylthiophen-2-yl)quinoxaline-5,8-diyl)dithiazole (TzQx)

4,7-di(thiazol-2-yl)benzo[c][1,2,5]thiadiazole (110 mg, 0.36mmol) and zinc dust (290 mg, 4.4 mmol) were added to a mixture of acetic acid (10 mL), ethanol (2.5 mL) and water (2.5

mL) and heated to 100°C under argon for 3 hours. The insoluble solid was then removed by filtration and the filtrate was added to 1,2-bis(5-octylthiophen-2-yl)ethane-1,2-dione (186 mg, 0.41 mmol). The mixture was heated at 65°C for 15 h. The organic compound was concentrated and purified by chromatography over silica with 10 % of ethyl acetate in C_6H_{14} as eluent. Finally, TzQx was obtained as an orange solid (172 mg, 69%). ^{1}H NMR ($CDCl_3$, 400 MHz, δ): 8.87 (s, 2H), 8.03 (d, *J* = 3.2 Hz, 2H), 7.61 (d, *J* = 3.2 Hz, 2H), 7.45 (d, *J* = 3.6 Hz, 2H), 6.75 (d, *J* = 3.6 Hz, 2H), 2.92 (t, *J* = 7.6 Hz, 4H), 1.78 (quint, *J* = 7.6 Hz, 4H), 1.5-1.2 (m, 20H), 0.90 (m, 6H); ^{13}C NMR ($CDCl_3$, 101 MHz, δ): 161.3, 151.6, 145.8, 142.3, 138.5, 136.1, 130.9, 130.7, 128.2, 124.8, 123.1, 31.9, 31.5, 30.4, 29.35, 29.27, 29.2, 22.7 and 14.1. Anal. Calcd for $C_{38}H_{44}N_4S_4$: C, 66.63; H, 6.47; N, 8.18; S, 18.72. Found: C, 66.56; H, 6.49; N, 7.99; S, 18.25. MS: calcd, 685.25216; found, 685.2522.

2,2'-(2,3-bis(5-octylthiophen-2-yl)quinoxaline-5,8-diyl)bis(5-bromothiazole)(TzQx-Br)

N-bromosuccinimide (55 mg, 0.31 mmol) was added on a solution of 2,2'-(2,3-bis(5-octylthiophen-2-yl)quinoxaline-5,8-diyl)dithiazole (105 mg, 0.15 mmol) in $CHCl_3$ (10 mL) and acetic acid (1.5 mL) at 0°C. The temperature slowly increased to room temperature. After 15 hours, the organic compound was concentrated and purified by chromatography over silica with 10 % of ethyl acetate in C_6H_{14} as eluent. Finally, TzQx-Br was obtained as an orange solid (120 mg, 93%). ^{1}H NMR ($CDCl_3$, 400 MHz, δ): 8.73 (s, 2H), 7.88 (s, 2H), 7.42 (d, *J* = 3.8 Hz, 2H), 6.77 (d, *J* = 3.8 Hz, 2H), 2.94 (t, *J* = 7.6 Hz, 4H), 1.80 (quint , *J* = 7.2 Hz, 4H), 1.5-1.2 (m, 20H), 0.89 (m, 6H); ^{13}C NMR ($CDCl_3$, 101 MHz, δ): 162.0, 152.1, 146.3, 143.5, 138.1, 135.8, 131.0, 127.4, 125.0, 113.8, 31.9, 31.5, 30.4, 29.4, 29.24, 29.18, 22.7 and 14.1. Anal. Calcd for $C_{40}H_{42}N_4S_4Br_2$: C, 54.15; H, 5.02; Br, 18.96; N, 6.65; S, 15.22. Found: C, 50.47; H, 4.97; N, 5.91; S, 13.56. MS: calcd, 841.07318; found, 841.0731.

General polymerization procedure

PDBS-TQx, **PDBS-TQxF** and **PDBS-TzQx** copolymers were synthesized by Suzuki coupling reaction. 5,5-dihexyl-3,7-bis(4,4,5,5-tetramethyl-1,3,2-dioxaborolan-2-yl)-5H-dibenzo[b,d]silole and the corresponding bis(bromo)-substituted quinoxaline monomer were solubilized in a mixture of toluene and DMF under argon. The mixture was degazed by freeze-thaw-pump. Then, tris(dibenzylideneacetone)dipalladium and tri-*tert*-butylphosphonium tetrafluoroborate were added. A 0.5M solution of K_2CO_3 in water was degased by bubbling argon in it during 15 hours, before adding. The schlenk was deeped in a thermostated oil bath at 95°C and kept under argon. After 28 hours, phenylboronic acid was added. After 1 hour, 2-bromothiophene was added. After 1 hour, the temperature was decreased to room temperature. The polymer was precipitated in methanol at 0°C and collected by filtration. The polymer purification included two steps. The polymer was dissolved in $CHCl_3$ (5 mL) at 60°C. Then deionized water (100 mL) and sodium diethyl-dithiocarbamate (1 g, 4.44 mmol) was added. The mixture was stirred vigorously at reflux overnight. The polymer was extracted into $CHCl_3$, the organic layer was washed with water, dried over $MgSO_4$ and concentrated. Finally, the polymer was precipitated in methanol and collected by filtration. The precipitate was Soxhlet extracted in order with cyclohexane and chloroform. The chloroform solution was concentrated to a small volume and precipitated into methanol. Finally, the polymer was collected by filtration and dried under vacuum overnight.

Poly(5-(5-(5,5-dihexyl-5H-dibenzo[b,d]silol-3-yl)thiophen-2-yl)-2,3-bis(5-octylthiophen-2-yl)-8-(thiophen-2-yl)quinoxaline) (PDBS-TQx)

For this polymerization 5,5-dihexyl-3,7-bis(4,4,5,5-tetramethyl-1,3,2-dioxaborolan-2-yl)-5H-dibenzo[b,d]silole (399 mg, 0.66 mmol), 5,8-bis(5-bromothiophen-2-yl)-2,3-bis(5-octylthiophen-2-yl)quinoxaline (530 mg, 0.63 mmol), tris(dibenzylideneacetone)dipalladium (11.5 mg, 12 µmol), tri-*tert*-butylphosphonium tetrafluoroborate (14.6 mg, 0.05 mmol), aqueous solution of K_2CO_3 (2.77 mL, 1.39 mmol) were solubilized in a mixture of toluene (13 mL) and DMF (7 mL). PDBS-TQx was obtained as a purple powder (258 mg, 40%). ^{1}H NMR ($CDCl_3$, 400 MHz, δ): 8.0-6.5 (Aromatic protons), 3.0-0.2 (Aliphatic protons). M_n = 48.8 kg.mol^{-1}, PDI = 3.3 (GPC, polystyrene calibration).

Poly(5-(5-(5,5-dihexyl-5H-dibenzo[b,d]silol-3-yl)thiophen-2-yl)-6,7-difluoro-2,3-bis(5-octylthiophen-2-yl)-8-(thiophen-2-yl)quinoxaline) (PDBS-TQxF)

For this polymerization 5,5-dihexyl-3,7-bis(4,4,5,5-tetramethyl-1,3,2-dioxaborolan-2-yl)-5H-dibenzo[b,d]silole (79 mg, 0.13 mmol), 5,8-bis(5-bromothiophen-2-yl)-6,7-difluoro-2,3-bis(5-octylthiophen-2-yl)quinoxaline (110 mg, 0.12 mmol), tris(dibenzylideneacetone)dipalladium (2.3 mg, 2.5 µmol), tri-*tert*-butylphosphonium tetrafluoroborate (2.9 mg, 0.01 mmol), aqueous solution of K_2CO_3 (0.55 mL, 0.28 mmol) were solubilized in a mixture of toluene (10 mL) and DMF (2.5 mL). PDBS-TQxF was obtained as a purple powder (109 mg, 81%). ^{1}H NMR ($CDCl_3$, 400 MHz, δ): 8.2-6.5 (Aromatic protons), 3.0-0.6 (Aliphatic protons). ^{19}F NMR ($CDCl_3$, 400 MHz, δ): -129.75 (m). M_n = 34.2 kg.mol^{-1}, PDI = 2.0 (GPC, polystyrene calibration).

Poly(2-(2,3-bis(5-octylthiophen-2-yl)-8-(thiazol-2-yl)quinoxalin-5-yl)-5-(5,5-dihexyl-5H-dibenzo[b,d]silol-3-yl)thiazole) (PDBS-TzQx)

For this polymerization 5,5-dihexyl-3,7-bis(4,4,5,5-tetramethyl-1,3,2-dioxaborolan-2-yl)-5H-dibenzo[b,d]silole (95 mg, 0.16 mmol), 2,2'-(2,3-bis(5-octylthiophen-2-yl)quinoxaline-5,8-diyl)bis(2-bromothiazole (127 mg, 0.15 mmol), tris(dibenzylidene-acetone)dipalladium (2.8 mg, 3 µmol), tri-*tert*-butylphosphonium tetrafluoroborate (3.5 mg, 0.01 mmol), aqueous solution of K_2CO_3 (0.66 mL, 0.33 mmol) were solubilized in a mixture of toluene (6 mL) and DMF (2.5 mL). PDBS-TzQx was obtained as a purple powder (48 mg, 31%). ^{1}H NMR ($CDCl_3$, 400 MHz, δ): 9.0-6.6 (Aromatic protons), 3.2-0.6 (Aliphatic protons). M_n = 18.9 kg.mol^{-1}, PDI = 2.2 (GPC, polystyrene calibration).

Physicochemical characterizations

UV-Vis absorption spectra were recorded on a Perkin-Elmer Lambda 2 spectrometer (wavelength range: 250–800 nm;

resolution: 2 nm). Electrochemical studies of the synthesized molecules were carried out in a one compartment, three-electrode electrochemical cell equipped with a flat platinum working electrode (7 mm^2), a Pt wire counter electrode, and a reference electrode of Ag/AgCl, whose potential was checked using the Fc/Fc^+ couple as an internal standard. The electrolyte consisted of 0.1 M tetrabutylammonium hexafluorophosphate (Bu_4NPF_6) solution in acetonitrile.

Organic field effect transistor devices preparation

Bottom contact field-effect transistors were elaborated on commercially available pre-patterned test structures whose source and drain contacts were composed of 30 nm thick gold and 10 nm thick Indium Tin Oxide (ITO) bilayers. A 230 nm thick silicon oxide was used as gate dielectric and n-doped (3 x $10^{17}cm^{-3}$) silicon crystal as gate electrode. The channel length and channel width were 20 µm and 10 mm respectively. The test structures were cleaned in acetone and isopropyl alcohol and subsequently for 15 minutes in a ultra-violet ozone system. Then, hexamethyldisilazane (HMDS) was spin-coated (500 rpm for 5 s and then 4000 rpm for 50 s) under nitrogen ambient and followed by an annealing step at 130°C for 15 minutes. Finally, 5 $mg.mL^{-1}$ anhydrous chloroform polymer solutions were spin coated (1250 rpm for 60s and 2000 rpm for 120s) to complete the FET devices. The samples were then left overnight under vacuum (<10^{-6} mbar) to remove residual solvent traces. Both, the FET elaboration and characterizations were performed in nitrogen ambient.

Devices characterizations

Patterned ITO glass substrates were cleaned using sequential sonication in water, acetone and isopropanol. The washed substrates were treated with a UV-ozone cleaner for 30 min, then, the hole transporting PEDOT:PSS (40nm) was spin-coated on the ITO glass, and dried at 180 °C for 30 min. Polymer and $PC_{71}BM$ in chlorobenzene were spin-coated to the substrate in a glove box 1,8-diodooctane (DIO) was used as a processing additive to optimized the morphology. Calcium (20nm) and Aluminium layers (100nm) were deposited by thermal evaporation under vacuum (10^{-7} mbar). The active area of the device was 0.28 cm². The current density-voltage characteristics of the devices in the dark and under white light illumination were measured using an AM 1.5G solar simulator. Current–voltage, I–V, characteristics and PCEs of the solar cells, illuminated through the ITO, were measured in inert atmosphere via a computer controlled Keithley 1 SMU 2400 unit using 100 $mW.cm^2$ airmass (1.5)-simulated white light generated by a Oriel SP94023A (Xe Lamp) Solar simulator. These simulated conditions are consistent with most published works to date. A monocrystalline silicon solar cell, calibrated at the Fraunhofer Institut Solare Energiesysteme (Freiburg, Germany), was used as a reference cell to confirm stabilization of the 100 $mW.cm^2$ illumination.

Acknowledgements

This work was financially supported by ANR through the Tandori research project no. ANR-11-PRGE-0011. RD and FC are grateful to Yann Kervella for the synthesis of some intermediates. Dr. Pascale Maldivi and Clément Thomassé as acknowledged for their help in the preparation or realization of some calculations and characterizations.

Contributions

F.C performed the synthesis and the characterization of the materials and the DFT calculations. He fabricated and characterized the solar cells and treated the data. N.D and P.C synthesized some of the precursors. P.L carried out the fabrication and the characterizations of the OFET. D.D and J.P performed the XRD measurements. J.F.V and N. Lemaitre contributed to the fabrication and the characterizations of the solar cells. B.G performed the morphology study of the blends with AFM and nc-AFM. J.P.T supervised the work. N. Leclerc and R.D supervised the work, designed the materials and the experiments, contributed to the analysis of the data and wrote the paper. All the authors revised the manuscript.

References

1 G. Yu, J. Gao, J. C. Hummelen, F. Wudl and A. J. Heeger, *Science*, 1995, **270**, 1789–1790.
2 K. A. Mazzio and C. K. Luscombe, *Chem Soc Rev*, 2015, **44**, 78–90.
3 L. Leonat, M. S. White, E. D. Głowacki, M. C. Scharber, T. Zillger, J. Rühling, A. Hübler and N. S. Sariciftci, *J. Phys. Chem. C*, 2014, **118**, 16813–16817.
4 G. Li, R. Zhu and Y. Yang, *Nat. Photonics*, 2012, **6**, 153–161.
5 S. Günes, H. Neugebauer and N. S. Sariciftci, *Chem. Rev.*, 2007, **107**, 1324–1338.
6 N. Blouin, A. Michaud and M. Leclerc, *Adv. Mater.*, 2007, **19**, 2295–2300.
7 Y. Liang, Z. Xu, J. Xia, S.-T. Tsai, Y. Wu, G. Li, C. Ray and L. Yu, *Adv. Mater.*, 2010, **22**, E135–E138.
8 D. H. Wang, J. K. Kim, J. H. Seo, I. Park, B. H. Hong, J. H. Park and A. J. Heeger, *Angew. Chem. Int. Ed.*, 2013, **52**, 2874–2880.
9 J. Y. Kim, K. Lee, N. E. Coates, D. Moses, T.-Q. Nguyen, M. Dante and A. J. Heeger, *Science*, 2007, **317**, 222–225.
10 J. Subbiah, B. Purushothaman, M. Chen, T. Qin, M. Gao, D. Vak, F. H. Scholes, X. Chen, S. E. Watkins, G. J. Wilson, A. B. Holmes, W. W. H. Wong and D. J. Jones, *Adv. Mater.*, 2015, **27**, 702–705.
11 Y. Liu, J. Zhao, Z. Li, C. Mu, W. Ma, H. Hu, K. Jiang, H. Lin, H. Ade and H. Yan, *Nat. Commun.*, 2014, **5**, 5293.
12 J. Zhao, Y. Li, G. Yang, K. Jiang, H. Lin, H. Ade, W. Ma and H. Yan, *Nat. Energy*, 2016, **1**, 15027.
13 J. You, L. Dou, K. Yoshimura, T. Kato, K. Ohya, T. Moriarty, K. Emery, C.-C. Chen, J. Gao, G. Li and Y. Yang, *Nat. Commun.*, 2013, **4**, 1446.
14 C.-C. Chen, W.-H. Chang, K. Yoshimura, K. Ohya, J. You, J. Gao, Z. Hong and Y. Yang, *Adv. Mater.*, 2014, **26**, 5670–5677.
15 A. R. bin M. Yusoff, D. Kim, H. P. Kim, F. K. Shneider, W. J. da Silva and J. Jang, *Energy Env. Sci*, 2015, **8**, 303–316.
16 J. Zhang, Y. Zhang, J. Fang, K. Lu, Z. Wang, W. Ma and Z. Wei, *J. Am. Chem. Soc.*, 2015, **137**, 8176–8183.
17 Y. Zhang, D. Deng, K. Lu, J. Zhang, B. Xia, Y. Zhao, J. Fang and Z. Wei, *Adv. Mater.*, 2015, **27**, 1071–1076.

18 L. Yang, L. Yan and Wei You, *J. Phys. Chem. Lett.*, 2013, **4**, 1802–1810.
19 C. Cabanetos, A. E. Labban, J. A. Bartelt, J. D. Douglas, W. R. Mateker, J. M. J. Fréchet, M. D. McGehee and P. M. Beaujuge, *J. Am. Chem. Soc.*, 2013, **135**, 4656–4659.
20 I. Osaka, T. Kakara, N. Takemura, T. Koganezawa and K. Tamimiya, *J. Am. Chem. Soc.*, 2013, **135**, 8834–8837.
21 S. H. Park, A. Roy, S. Beaupré, S. Cho, N. Coates, J. S. Moon, D. Moses, M. Leclerc, K. Lee and A. J. Heeger, *Nat. Photonics*, 2009, **3**, 297–302.
22 T. Ameri, N. Li and C. J. Brabec, *Energy Environ. Sci.*, 2013, **6**, 2390.
23 J. You, L. Dou, Z. Hong, G. Li and Y. Yang, *Prog. Polym. Sci.*, 2013, **38**, 1909–1928.
24 J. Gilot, M. M. Wienk and R. A. J. Janssen, *Adv. Mater.*, 2010, **22**, E67–E71.
25 L. Huo, T. Liu, X. Sun, Y. Cai, A. J. Heeger and Y. Sun, *Adv. Mater.*, 2015, **27**, 2938–2944.
26 G. Zhao, Y. He and Y. Li, *Adv. Mater.*, 2010, **22**, 4355–4358.
27 S. Beaupré and M. Leclerc, *J. Mater. Chem. A*, 2013, **1**, 11097.
28 J. Wolf, F. Cruciani, A. El Labban and P. M. Beaujuge, *Chem. Mater.*, 2015, **27**, 4184–4187.
29 A. Cravino, *Appl. Phys. Lett.*, 2007, **91**, 243502.
30 H. Zhou, L. Yang and W. You, *Macromolecules*, 2012, **45**, 607–632.
31 J. Chen and Y. Cao, *Acc. Chem. Res.*, 2009, **42**, 1709–1718.
32 J. Zhang, W. Cai, F. Huang, E. Wang, C. Zhong, S. Liu, M. Wang, C. Duan, T. Yang and Y. Cao, *Macromolecules*, 2011, **44**, 894–901.
33 A. Tournebize, P.-O. Bussière, P. Wong-Wah-Chung, S. Thérias, A. Rivaton, J.-L. Gardette, S. Beaupré and M. Leclerc, *Adv. Energy Mater.*, 2013, **3**, 478–487.
34 M. Jørgensen, K. Norrman, S. A. Gevorgyan, T. Tromholt, B. Andreasen and F. C. Krebs, *Adv. Mater.*, 2012, **24**, 580–612.
35 R. Kroon, A. Lundin, C. Lindqvist, P. Henriksson, T. T. Steckler and M. R. Andersson, *Polymer*, 2013, **54**, 1285–1288.
36 H.-C. Chen, Y.-H. Chen, C.-H. Liu, Y.-H. Hsu, Y.-C. Chien, W.-T. Chuang, C.-Y. Cheng, C.-L. Liu, S.-W. Chou, S.-H. Tung and P.-T. Chou, *Polym. Chem.*, 2013, **4**, 3411.
37 D. Dang, W. Chen, R. Yang, W. Zhu, W. Mammo and E. Wang, *Chem. Commun.*, 2013, **49**, 9335.
38 N. Leclerc, P. Chávez, O. A. Ibraikulov, T. Heiser and P. Lévêque, *Polymers*, 2016, **8**.
39 J.-H. Kim, C. E. Song, H. U. Kim, A. C. Grimsdale, S.-J. Moon, W. S. Shin, S. K. Choi and D.-H. Hwang, *Chem. Mater.*, 2013, **25**, 2722–2732.
40 P. Yang, M. Yuan, D. F. Zeigler, S. E. Watkins, J. A. Lee and C. K. Luscombe, *J Mater Chem C*, 2014, **2**, 3278–3284.
41 H. Zhou, L. Yang, A. C. Stuart, S. C. Price, S. Liu and W. You, *Angew. Chem. Int. Ed.*, 2011, **50**, 2995–2998.
42 E. Zaborova, P. Chávez, R. Bechara, P. Lévêque, T. Heiser, S. Méry and N. Leclerc, *Chem. Commun.*, 2013, **49**, 9938.
43 K. L. Chan, M. J. McKiernan, C. R. Towns and A. B. Holmes, *J. Am. Chem. Soc.*, 2005, **127**, 7662–7663.
44 M. Svensson, F. Zhang, S. C. Veenstra, W. J. H. Verhees, Jan C. Hummelen, J. M. Kroon, O. Inganäs and M. R. Andersson, *Adv. Mater.*, 2003, **15**, 988–991.
45 S. Li, Z. He, J. Yu, S. Chen, A. Zhong, H. Wu, C. Zhong, J. Qin and Z. Li, *J. Polym. Sci. Part Polym. Chem.*, 2012, **50**, 2819–2828.
46 Z. Li, J. Lu, S.-C. Tse, J. Zhou, X. Du, Y. Tao and J. Ding, *J. Mater. Chem.*, 2011, **21**, 3226.
47 P. Chavez, C. Ngov, P. de Frémont, P. Lévêque and N. Leclerc, *J. Org. Chem.*, 2014, **79**, 10179–10188.
48 Y.-J. Cheng, S.-H. Yang and C.-S. Hsu, *Chem. Rev.*, 2009, **109**, 5868–5923.
49 Y. Kim, H. R. Yeom, J. Y. Kim and C. Yang, *Energy Environ. Sci.*, 2013, **6**, 1909.
50 I. Polec, A. Henckens, L. Goris, M. Nicolas, M. A. Loi, P. J. Adriaensens, L. Lutsen, J. V. Manca, D. Vanderzande and N. S. Sariciftci, *J. Polym. Sci. Part Polym. Chem.*, 2003, **41**, 1034–1045.
51 X. Gong, M. Tong, F. G. Brunetti, J. Seo, Y. Sun, D. Moses, F. Wudl and A. J. Heeger, *Adv. Mater.*, 2011, **23**, 2272–2277.
52 J. Hou, T. L. Chen, S. Zhang, L. Huo, S. Sista and Y. Yang, *Macromolecules*, 2009, **42**, 9217–9219.
53 J.-M. Verilhac, G. LeBlevennec, D. Djurado, F. Rieutord, M. Chouiki, J.-P. Travers and A. Pron, *Synth. Met.*, 2006, **156**, 815–823.
54 R. Noriega, J. Rivnay, K. Vandewal, F. P. V. Koch, N. Stingelin, P. Smith, M. F. Toney and A. Salleo, *Nat. Mater.*, 2013, **12**, 1038–1044.
55 A. Salleo, *Mater. Today*, 2007, **10**, 38–45.
56 P. Liu, K. Zhang, F. Liu, Y. Jin, S. Liu, T. P. Russell, H.-L. Yip, F. Huang and Y. Cao, *Chem. Mater.*, 2014, **26**, 3009–3017.
57 J. Sakai, K. Kawano, T. Yamanari, T. Taima, Y. Yoshida, A. Fujii and M. Ozaki, *Sol. Energy Mater. Sol. Cells*, 2010, **94**, 376–380.
58 C. Sprau, F. Buss, M. Wagner, D. Landerer, M. Koppitz, A. Schulz, D. Bahro, W. Schabel, P. Scharfer and A. Colsmann, *Energy Env. Sci*, 2015, **8**, 2744–2752.
59 J. Peet, J. Y. Kim, N. E. Coates, W. L. Ma, D. Moses, A. J. Heeger and G. C. Bazan, *Nat. Mater.*, 2007, **6**, 497–500.
60 K. Schmidt, C. J. Tassone, J. R. Niskala, A. T. Yiu, O. P. Lee, T. M. Weiss, C. Wang, J. M. J. Fréchet, P. M. Beaujuge and M. F. Toney, *Adv. Mater.*, 2014, **26**, 300–305.
61 P. Westacott, J. R. Tumbleston, S. Shoaee, S. Fearn, J. H. Bannock, J. B. Gilchrist, S. Heutz, J. deMello, M. Heeney, H. Ade, J. Durrant, D. S. McPhail and N. Stingelin, *Energy Environ. Sci.*, 2013, **6**, 2756.
62 F. Fuchs, F. Caffy, R. Demadrille, T. Mélin and B. Grévin, *ACS Nano*, 2016, **10**, 739–746.
63 S. R. Cowan, A. Roy and A. J. Heeger, *Phys. Rev. B*, 2010, **82**, 245207.
64 L. J. A. Koster, V. D. Mihailetchi, R. Ramaker and P. W. M. Blom, *Appl. Phys. Lett.*, 2005, **86**, 123509.
65 Y. Deng, W. Li, L. Liu, H. Tian, Z. Xie, Y. Geng and F. Wang, *Energy Env. Sci*, 2015, **8**, 585–591.
66 A. K. K. Kyaw, D. H. Wang, D. Wynands, J. Zhang, T.-Q. Nguyen, G. C. Bazan and A. J. Heeger, *Nano Lett.*, 2013, **13**, 3796–3801.
67 L. J. A. Koster, M. Kemerink, M. M. Wienk, K. Maturová and R. A. J. Janssen, *Adv. Mater.*, 2011, **23**, 1670–1674.
68 S. Albrecht, S. Janietz, W. Schindler, J. Frisch, J. Kurpiers, J. Kniepert, S. Inal, P. Pingel, K. Fostiropoulos, N. Koch and D. Neher, *J. Am. Chem. Soc.*, 2012, **134**, 14932–14944.

Scheme 1. Synthetic routes of the monomers TQx, TQxF and TzQx.

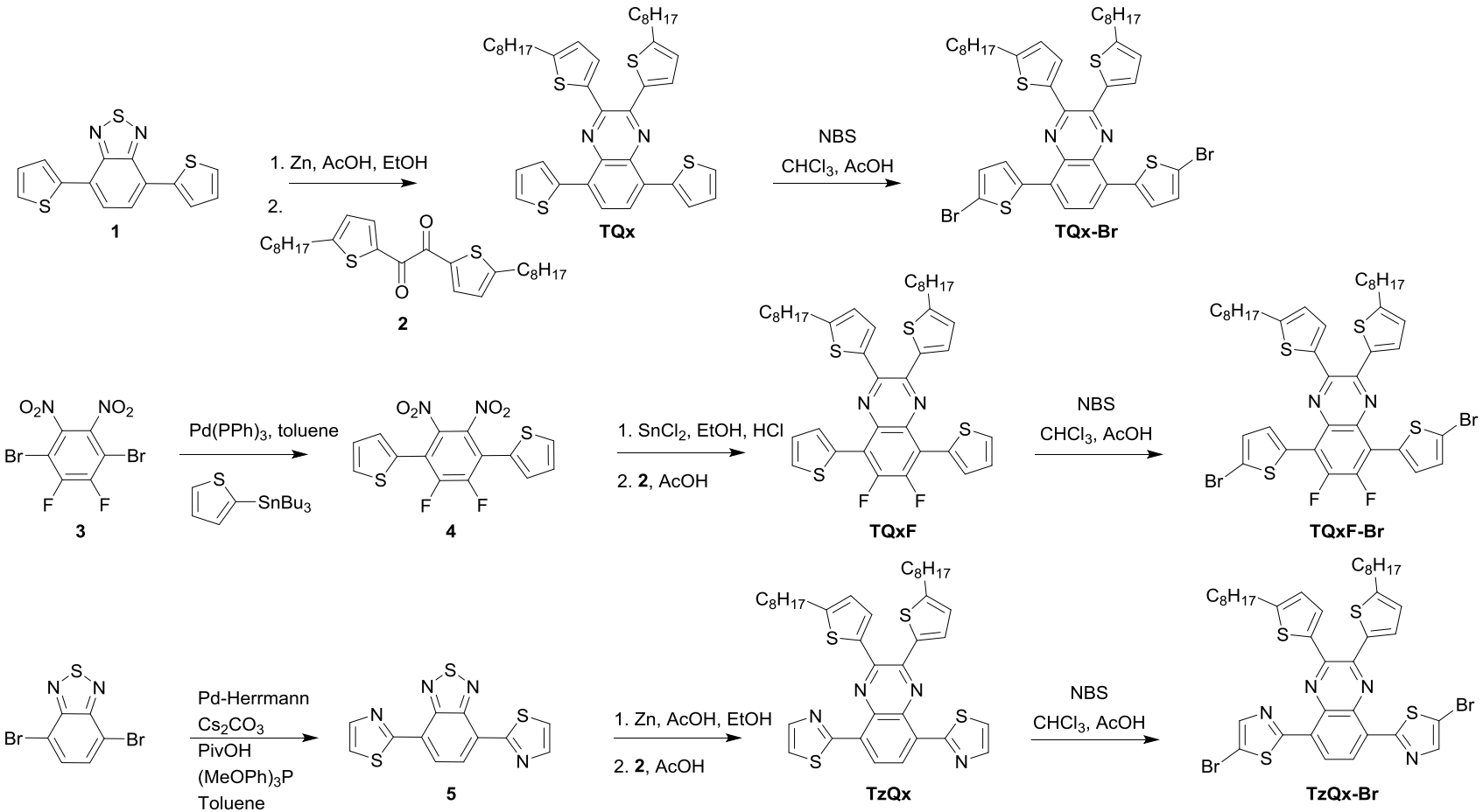

Scheme 2. Synthetic routes of the polymers PDBS-TQx, PDBS-TQxF and PDBS-TzQx.

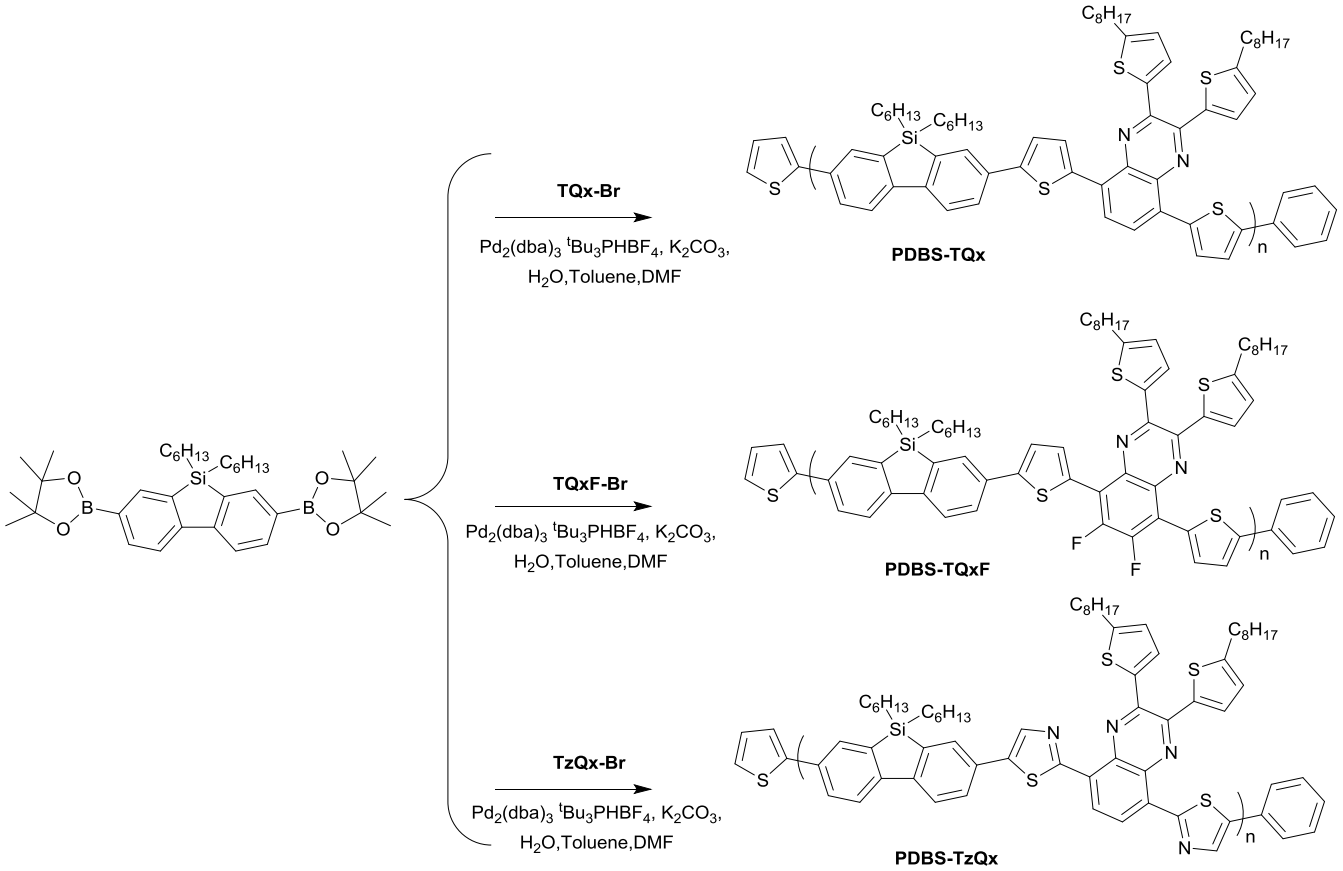

Figure 1. (a) UV-Visible absorption spectra of PDBS-TQx, PDBS-TQxF and PDBS-TzQx in solution in chloroform. (b) in thin films.

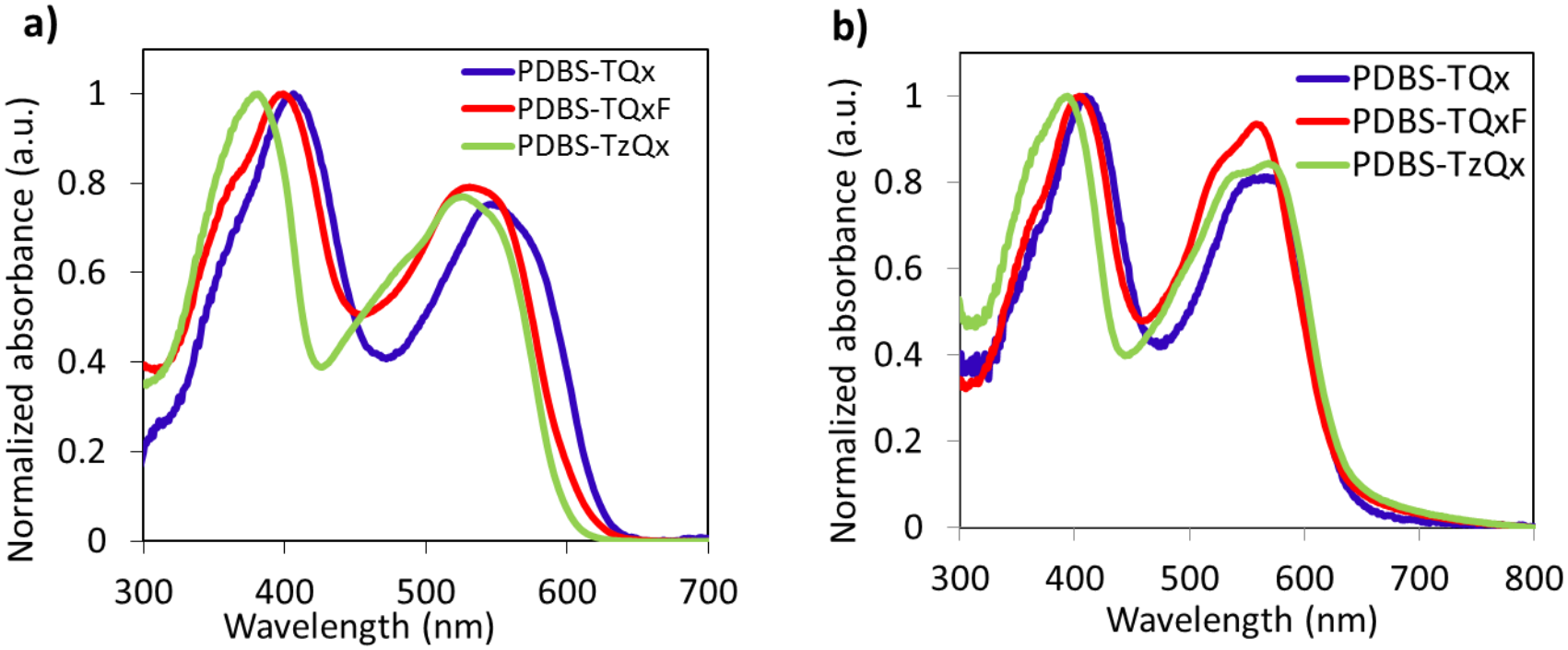

Figure 2. X-Ray diffraction patterns of polymers PDBS-TQx, PDBS-TQxF and PDBS-TzQx in films.

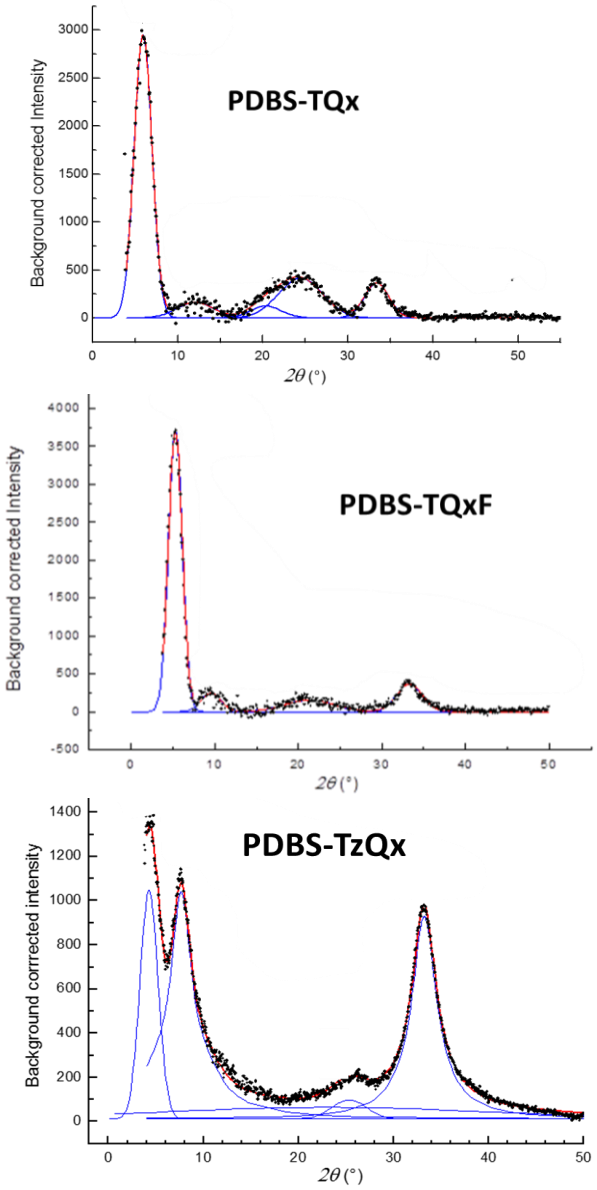

Table 1 Angular positions of the Bragg peaks and periodical distances measured by X-ray diffraction of PDBS-TQx, PDBS-TQxF and PDBS-TzQx polymers in films.

Polymers	Angle 2θ (°)	Distance (Å)
PDBS-TQx	5.94	17.33
	12.20	8.52
	20.14	5.07
	24.47	4.23
PDBS-TQxF	5.42	19.34
	9.54	10.71
	21.44	4.83
PDBS-TzQx	4.97	23.93
	7.77	13.39
	24.94	4.14

Table 2 Optical and eletrochemical properties of PDBS-TQx, PDBS-TQxF and PDBS-TzQx

Polymers	$\lambda_{max,sol}$ (nm)	$\lambda_{max,\ film}$ (nm)	$\lambda\ edge_{film}$ (nm)	$E_{gap,opt}$ (eV)	E_{OX} (V)	E_{RED} (V)	E_{HOMO} (eV)	E_{LUMO} (eV)	$E_{gap,elect}$ (eV)
PDBS-TQx	406, 546	410, 565	630	1.97	0.94	-1.27	-5.32	-3.11	2.21
PDBS-TQxF	396, 531	404, 558	631	1.96	1.09	-1.28	-5.47	-3.10	2.37
PDBS-TzQx	381, 526	394, 569	633	1.96	1.31	-1.11	-5.69	-3.27	2.42

Figure 3. (a) Cyclic voltammograms of the polymers PDBS-TQx, PDBS-TQxF and PDBS-TzQx. (b) HOMO and LUMO energy levels of the copolymers.

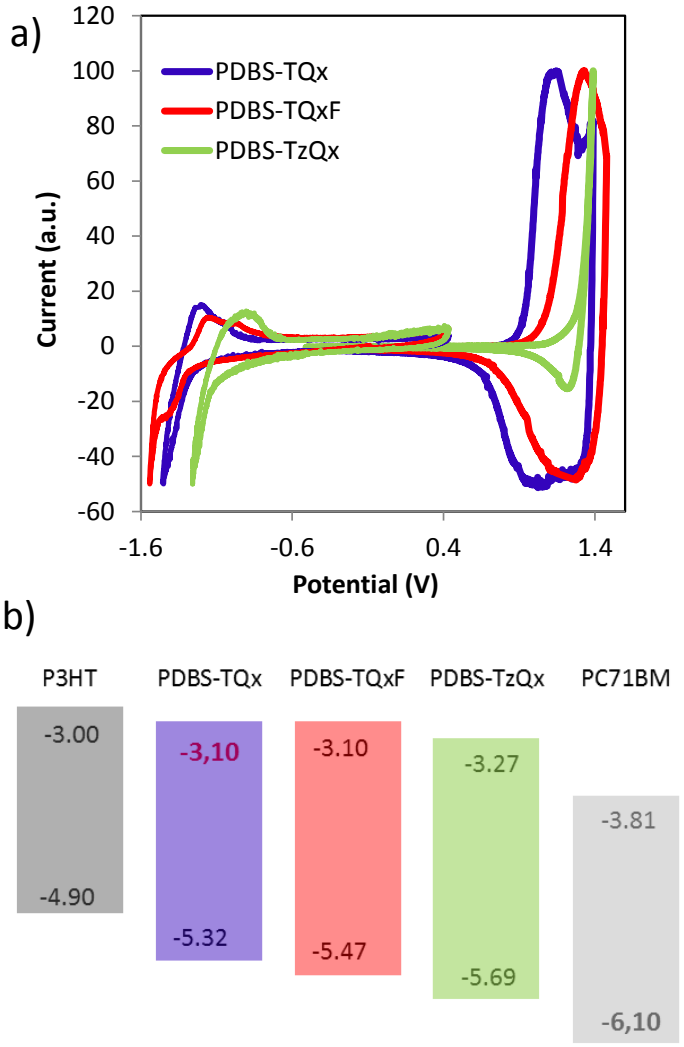

Figure 4. DFT calculated HOMO and LUMO wave functions of the geometry-optimized repeating unit structure PDBS-TQx, PDBS-TQxF and PDBS-TzQx.

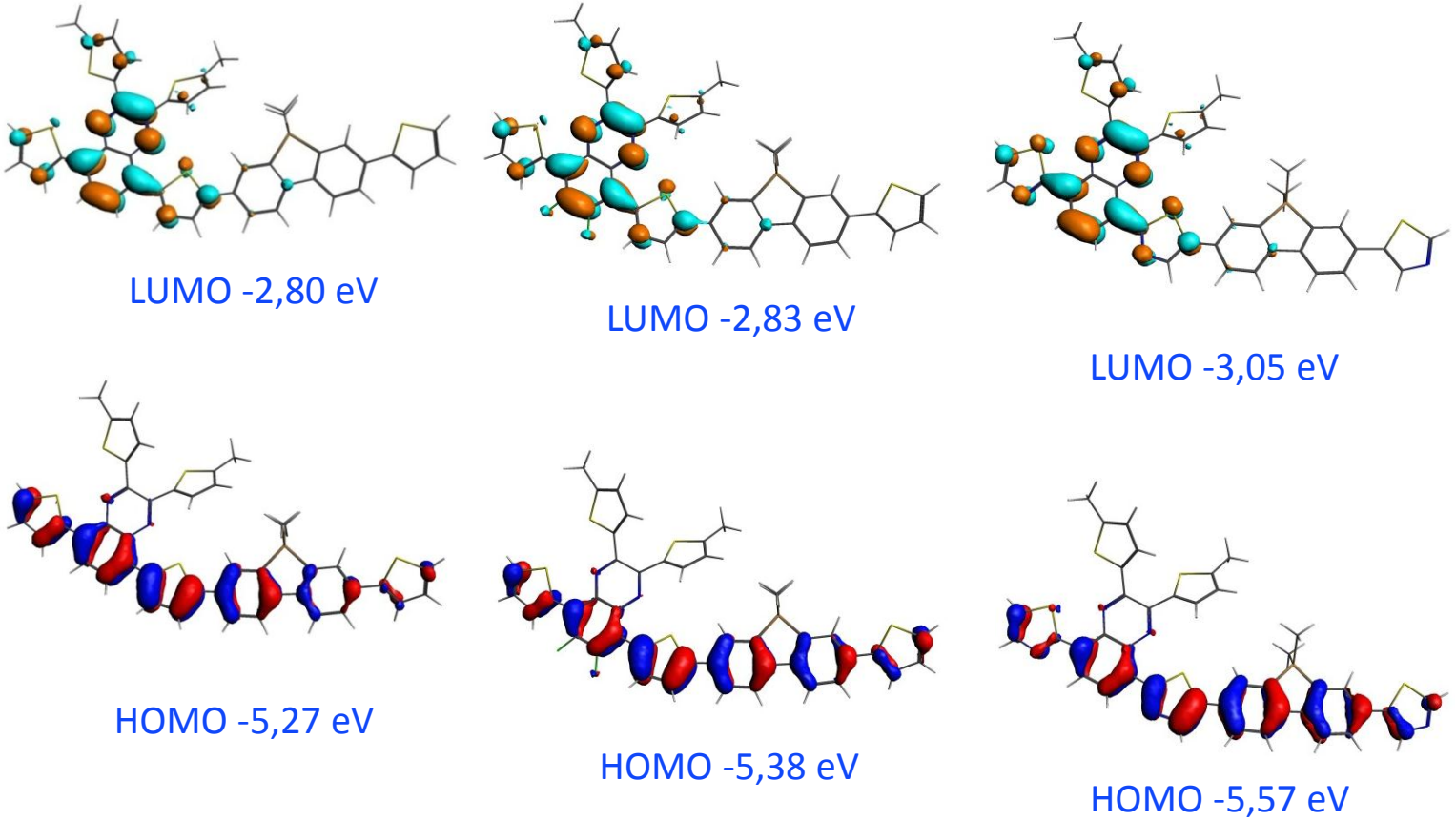

Table 3 Hole mobilities in Organic field-effect transistors of PDBS-TQx, PDBS-TQxF and PDBS-TzQx.

Polymer	As deposited		Annealed 100°C 10 min.	
	μ_{lin} ($cm^2.V^{-1}.s^{-1}$)	μ_{sat} ($cm^2.V^{-1}.s^{-1}$)	μ_{lin} ($cm^2.V^{-1}.s^{-1}$)	μ_{sat} ($cm^2.V^{-1}.s^{-1}$)
PDBS-TQx	$3.0x10^{-4}$	$8.5x10^{-4}$	$2.5x10^{-4}$	$4.5x10^{-4}$
PDBS-TQxF	$1.0x10^{-3}$	$2.0x10^{-3}$	$4.5x10^{-3}$	$6.5x10^{-3}$
PDBS-TzQx	$2.0x10^{-5}$	$8.0x10^{-5}$	$4.0x10^{-5}$	$1.5x10^{-4}$

Table 4 Photovoltaic properties BHJ PSCs of PDBS-TQx, PDBS-TQxF, PDBS-TzQx and P3HT. [a] Average on 5 solar cells (active area, 0.28cm²). [b] this work, [c] according to reference [57].

Active layer	Ratio	Solvent	Additive	Thickness (nm)	V_{OC} (V)	J_{SC} (mA.cm^{-2})	FF	PCE (%)
PDBS-TQx:$PC_{71}BM$	1:2	CB	3 % DIO	50	0.85	9.72	0.62	5.14 ([a]4.93)
PDBS-TQxF:$PC_{71}BM$	1:2	CB	3 % DIO	75	0.81	7.27	0.51	2.98 ([a]2.78)
PDBS-TzQx:$PC_{71}BM$	1:3	CB	3 % DIO	50	0.63	4.92	0.41	1.27 ([a]1.03)
P3HT:$PC_{61}BM$	1:0.8	o-DCB	no DIO	100	0.63	9.50	0.68	4.07[b]
P3HT:$PC_{71}BM$	1 :0.7	o-DCB	no DIO	200	0.64	11.30	0.58	4.21[c]

Figure 5. Current-density-voltage characteristics of optimized devices of PDBS-TQx, PDBS-TQxF and PDBS-TzQx.

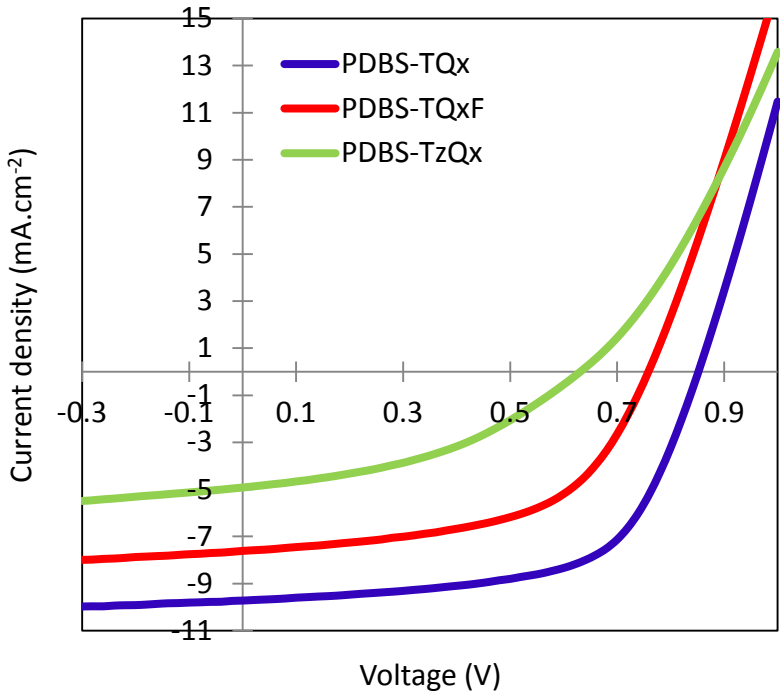

Figure 6. AFM images, topography, 3µm x 3 µm of active layer made of: (a) PDBS-TQx:$PC_{71}BM$ 1:2 (b) PDBS-TQx:$PC_{71}BM$ 1:2 + 3%DIO (c) PDBS-TQxF:$PC_{71}BM$ 1:2 (d) PDBS-TQxF:$PC_{71}BM$ 1:2 + 3%DIO (e) PDBS-TzQx:$PC_{71}BM$ 1:2 (f) PDBS-TzQx:$PC_{71}BM$ 1:2 + 3%DIO

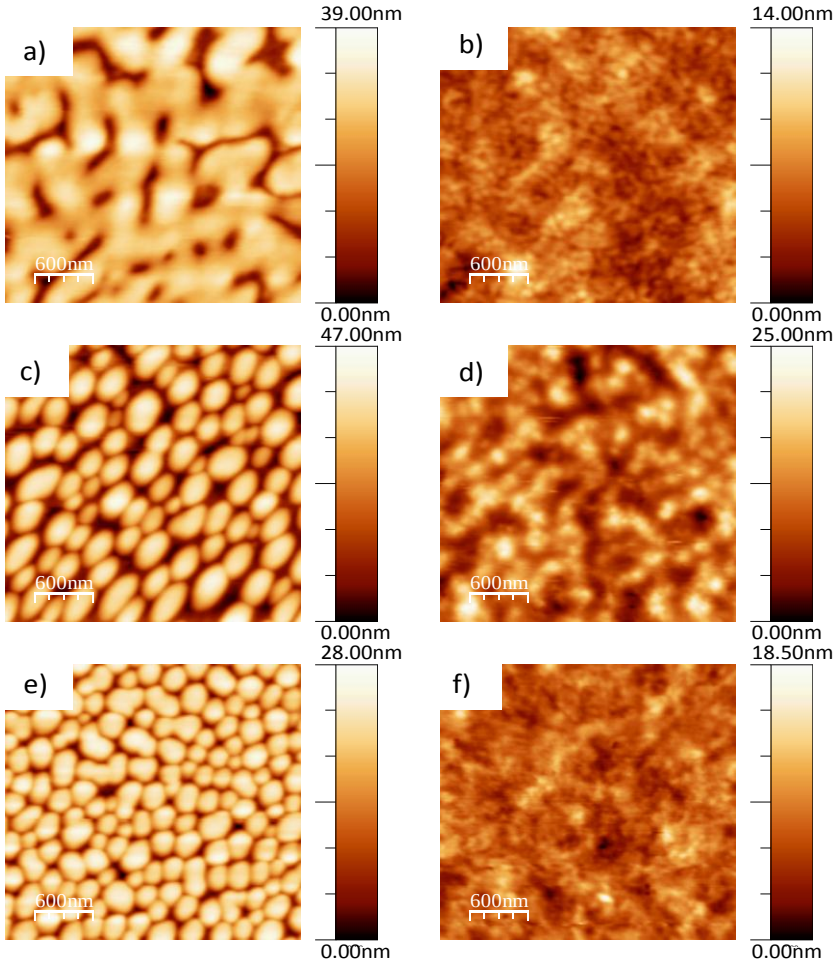

Figure 7. High resolution topographic (a) and damping (b,c) nc-AFM images of the blend PDBS-TQx:$PC_{71}BM$ in the dark. The white and yellow contours in (c) pinpoint nanometer and mesoscopic scale domains, respectively.

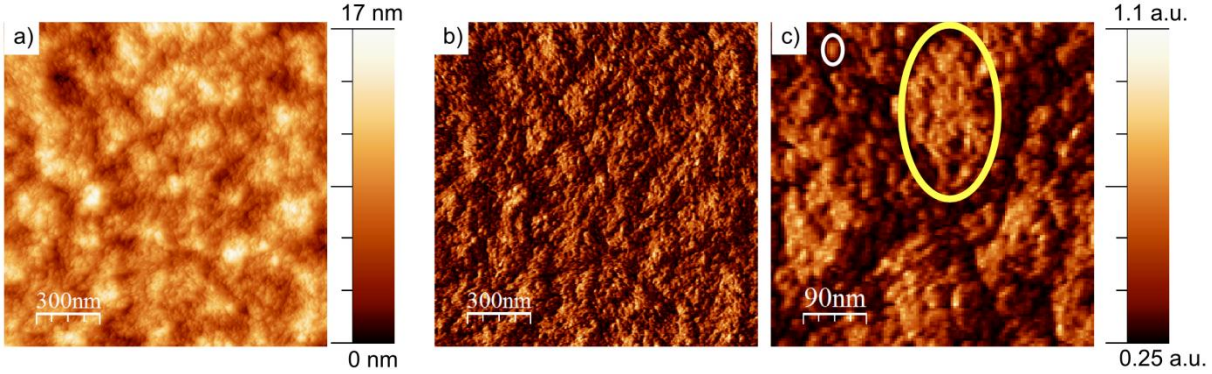

Figure 8. *J*-V curves for BHJ solar cells of PDBS-TQx:$PC_{71}BM$ 1:2 (a) and PDBS-TQxF:$PC_{71}BM$ 1:2 (b) under different light intensities.

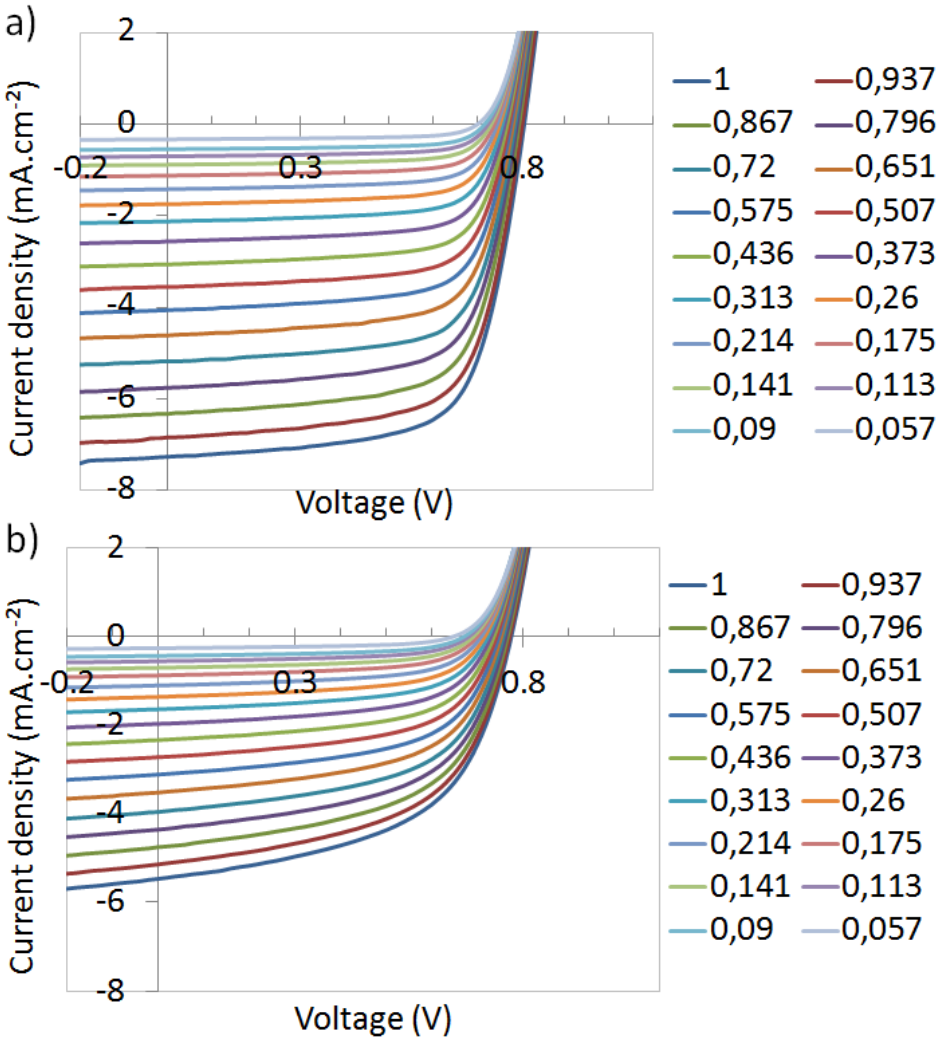

Figure 9. Double logarithmic plot of J_{SC} as a function of the light intensity and fitting line according to the power law.

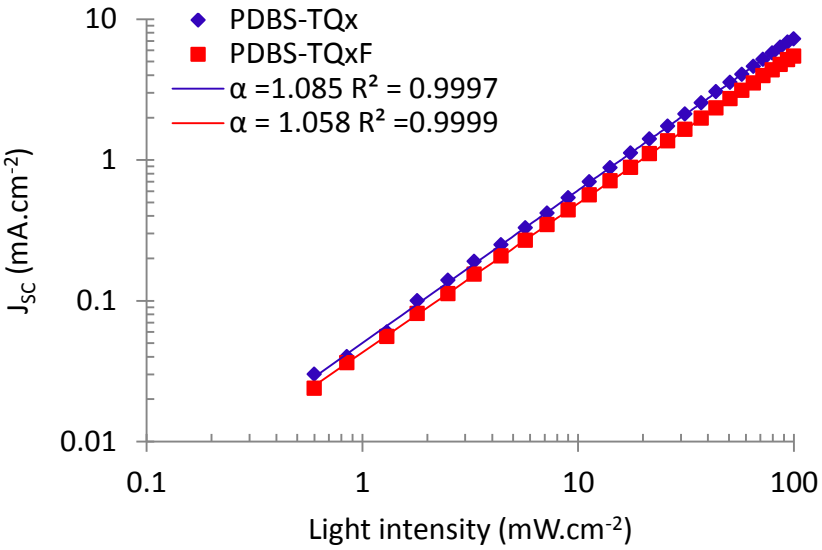

Figure 10. V_{OC} as a function of light intensity with linear fit.

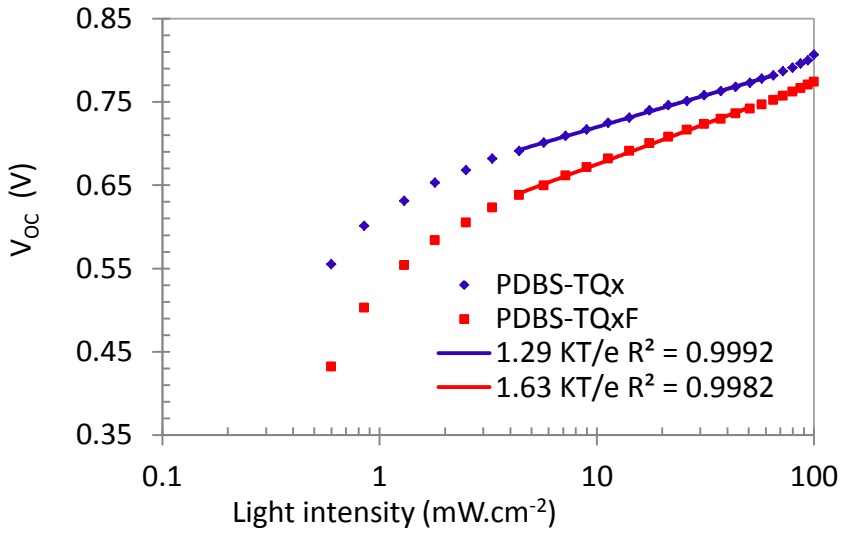

Dibenzosilole and quinoxaline based copolymers were synthesized and tested in bulk-heterojunction solar cells showing power conversion efficiencies up to 5.14%.

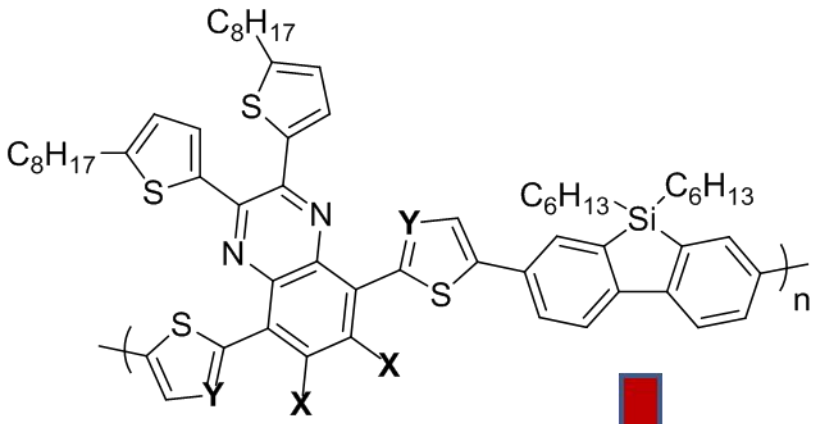

X= H or F

Y = CH or N

Wide Band-Gap copolymers

1,95 eV < Eg < 2 eV